U. S. DEPARTMENT OF THE INTERIOR
U. S. GEOLOGICAL SURVEY

A MODEL FOR GRAIN FLOW AND DEBRIS FLOW

by

Arvid M. Johnson[1]

Open–File Report 96–728

Prepared in Cooperation with Landslide Hazard Reduction Program
Denver, Colorado
1996

1 Former W.A.E. with U.S. Geological Survey, Denver, Colorado.
Geosciences Department, Purdue University, West Lafayette, Indiana 47907

Table of Contents

PAGE 5 FOLLOWS

ABSTRACT

This paper is a study of the rheology of shearing grain–flow and debris–flow materials. A general rheological model is developed that incorporates, simultaneously, the macro–viscous rheology we have developed for simple debris flows and the inertial rheology developed by Bagnold for grain flows. The combined model largely accounts for the dynamic behavior of spherical grains and water as measured by Bagnold (1954) and of mixtures of sand, water and clay, as measured under undrained conditions with a new apparatus, the rolling–sleeve viscometer. The model predicts the flow curves for sand–fluid mixtures and simple debris with interstitial slurries with various viscosities. It predicts the effects of wide ranges of concentrations of sand on the viscosities of sand–fluid mixtures and simple–debris.

The research reported here is a foundation for further research. The rheological model provides a basis for analyzing flows in which concentration of the granular phase changes from place to place, such as subaerial or subaqueous channel flow and for subaqueous turbidity flow. Some of these complexities are illustrated via numerical solutions of the equations governing the flow of the idealized material down a wide channel. We study solutions for end members of undrained flow and completely drained flow in order to bracket the range of possible behaviors of such mixtures.

INTRODUCTION

In a series of papers that have become classics in geological literature, Bagnold (1936, 1941, 1954, 1956, 1966, 1980) provided a sound foundation for investigations of the flow of granular materials, especially grain flows, in which the impact of interstitial grains is a major source of resistance to flow. Starting somewhat later, I (1965, 1970, 1984) developed macro–viscous rheological models (Terzaghi–Coulomb–viscous flow) for a special kind of flow of granular materials, debris flow (Figure 1and Figure 2), involving granular materials and clay–water slurries, in order to understand various field and experimental observations of debris flows. In macro–viscous flow, the resistance is a combination of the strength and viscosity of the slurry in the interstices of the coarser, granular phase and the interaction of the particles of the granular phase. A familiar material that moves by macro–viscous flow is wet concrete. If one wants to correctly think about how mobile debris would appear, one thinks about wet concrete, except it is a peculiar wet concrete in which the rock aggregate does not necessarily consist of granules and pebbles, but may include cobbles and even boulders. In contrast, in inertial flow analyzed by Bagnold, the material flows much like dry sand on a steep slope. The particles bang together, saltate and generally disperse as they move *en–masse*, down slope. A natural example—that must have flowed by this mechanism, except there certainly was interstitial water—produced the slugs of debris in deposits at Klare Springs in Death Valley (Figure 3).

I made no attempt to reconcile the two approaches until the 1970's, when Rodine and Johnson (1976) investigated the mechanism of strength of debris and McTigue (1979) re–investigated Bagnold's grain–inertia model for dry granular solids. On the basis of those studies, I suggested a general form for a rheological model for debris flow (Johnson, 1984), but did not pursue the matter.

These different investigations led, of course, to divergent conclusions about how debris moves and these have been the subject of some controversy. Several investigators have claimed that debris flows are identical to grain flows (e.g., Takahashi, 1991) or have mechanically analyzed debris flows by assuming that the inertial mechanisms of grain flow are the only relevant mechanisms of debris flow (Bagnold, 1956; Takahashi, 1977, 1980, 1991; Chen, 1985). My concurrent research had assumed that debris flow would be dominated by macro–viscous rheological properties (Johnson, 1965, 1970; Johnson and Hampton, 1968, 1969; Johnson and Rahn, 1970; Hampton, 1972), but it had migrated toward the Bagnoldian approach (McTigue, 1982; Rodine and Johnson, 1976; Johnson, 1984; Martosudarmo, 1994).

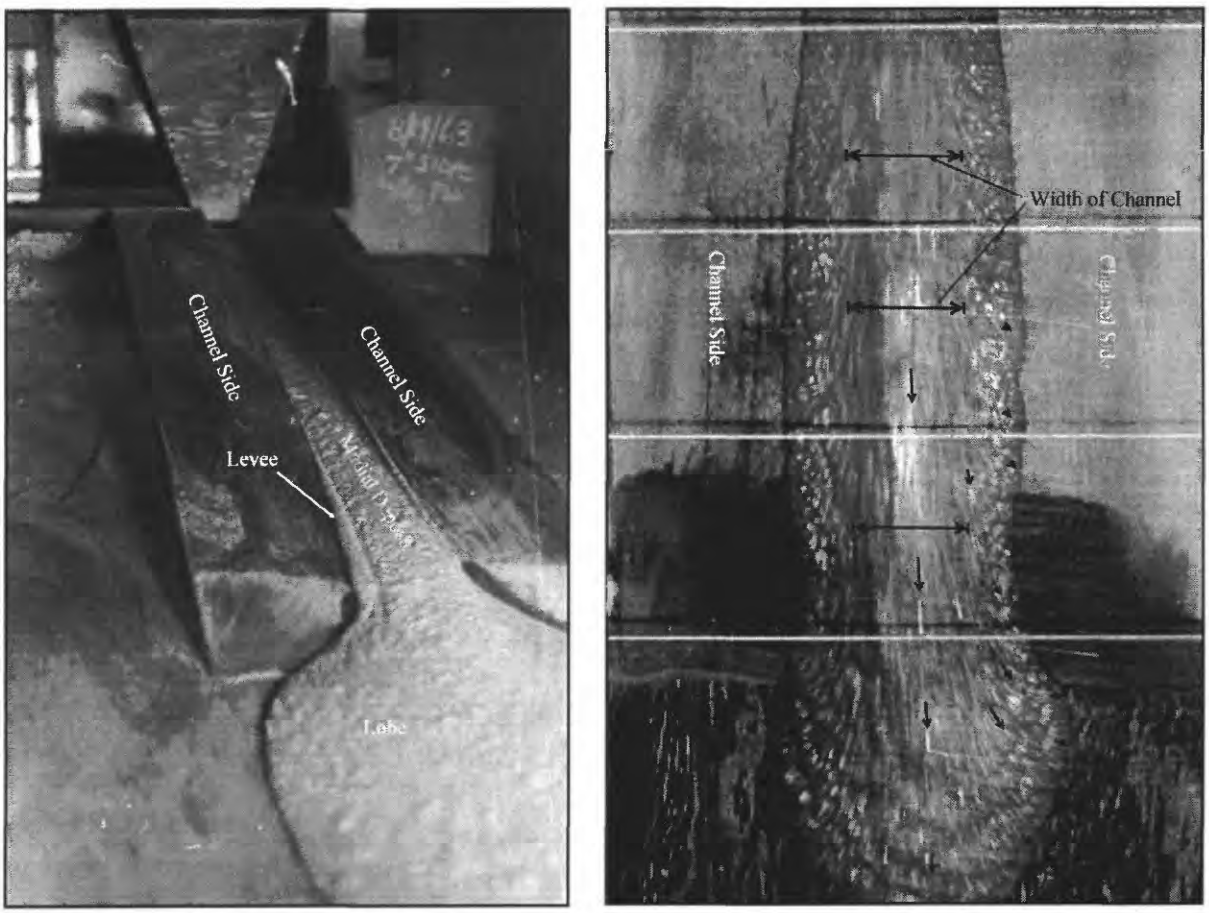

A. B.

Figure 1. Experimental debris flows moving down channel, about ten cm wide, and of decreasing depth distally. Debris is pebbly silt unit of 1917 Surprise Canyon debris flow deposit in Panamint Valley, California (Johnson, 1965). Debris contains water plus grains ranging from granules to clay sizes. A. Oblique view of debris chute source in distance, rectangular channel and planar "fan" in foreground, showing levee (or lateral deposit), medial deposit and lobe of a typical experiment. Slope angle of planar surface is 7°. B. Vertical view of moving flow at exposure time of about 1/30 sec. Traces are paths of reflective flakes of "glitter." Black, double–headed arrows show sides of channel, below mud surface. Mud outside these limits is in overbank, levee flow or deposit. Black single–headed arrows show, approximately, direction of horizontal component of velocity vectors at various places. The pattern shows how particles originally in center of channel end up in levees and in outer edge of snout of flow.

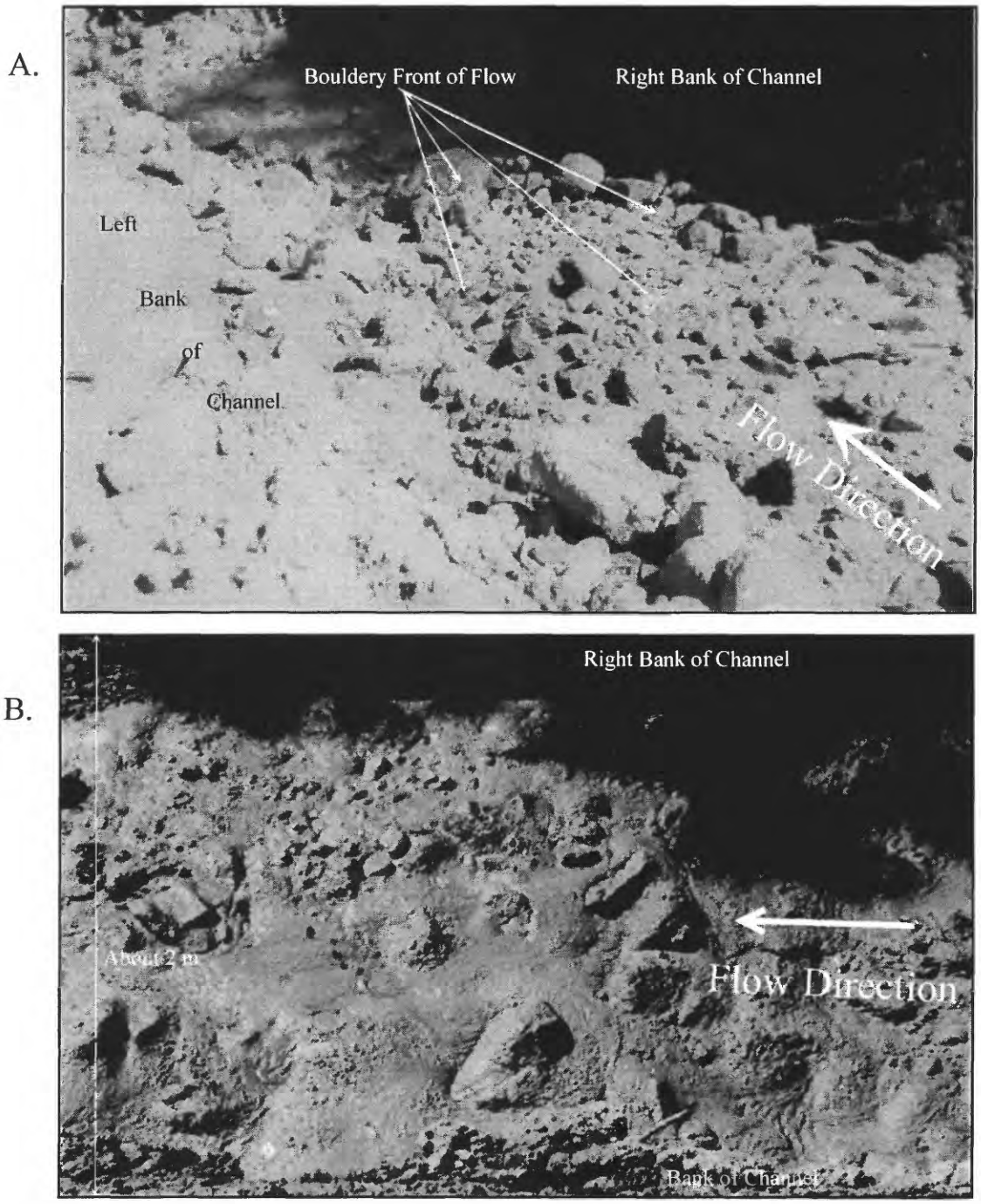

Figure 2. Two parts of a debris flow during 1969, Wrightwood, California debris–flow episode. A. Oblique view over top of front of debris flow, showing abundant large clasts protruding from the front, essentially forming a dam of interlocked blocks and boulders. Largest boulder about 50 cm in maximum dimension. B. High, oblique view of debris flow a few meters behind bouldery front, exposing more of the interstitial mud. The boulders appear to be more widely separated and to be smaller. Channel two to two and a half m wide. In later parts of this flow, the largest particles become smaller, and the flow becomes thinner. Eventually, the channel returns to a small stream of muddy water, until another debris flow appears (Johnson, 1970).

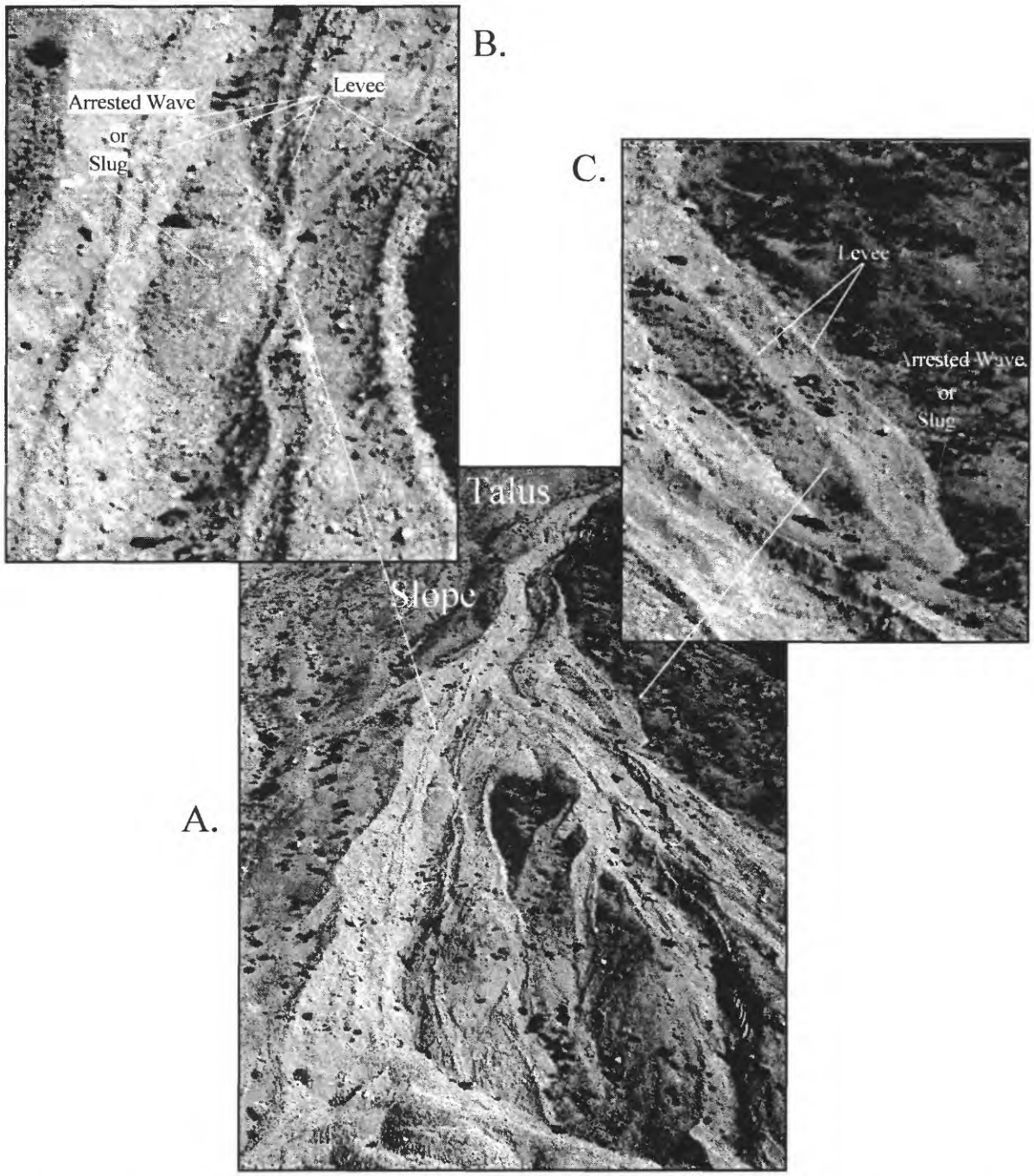

Figure 3. Avalanche or debris–flow deposits on a steep talus cone near Klare Springs, on south wall of Titus Canyon, Death Valley, California. A. Complex of deposits of many avalanche waves. Slope in foreground about 35°. In the vicinity of the arrested wave, the slope angle is about 25°. B. Detail of arrested wave, showing open, clean channel upstream and downstream from wave. Maximum width of arrested wave about 5 m. Channel roughly U–shaped and on sides are at least four pairs of levees, reflecting four waves that passed through channel. Each wave produced paired levees. C. Channel down which two waves moved. The levees are distinct, but the medial deposits are nil. The two arrested waves at the distal end can be distinguished only with difficulty. They are small because they have been largely depleted by materials left behind in levees, as described in pyroclastic–flow deposits at Mt. St. Helens by Schulz (1996).

The Bagnoldian approach of investigating fundamental mechanisms of flowing granular solids is valuable for many reasons. It describes rheological properties of debris in terms of fundamental variables related to its constituents, such as fluid viscosity and grain size, density and concentration, as has been advocated by Iverson and Denlinger (1987). Also, it is valuable because it predicts correctly the large contribution of the grains being transported to the gross viscosity of the mixture of transporting fluid and grains. Finally, it correctly predicts the variability of rheological properties of debris from place to place within a flow. Ironically, this latter prediction largely discredits the measurements that Bagnold and others have performed to study the dispersive–pressure phenomenon because rheology generally must be studied under constant–state conditions if one's conclusions are to be valid (Rivlin, 1947, 1948, 1951;Truesdell and Noll, 1965).

This paper attempts to unify the rheological research on grain flow, debris avalanche and debris flow by proposing a combined macro–viscous and inertial model and using experimental measurements that we have recently made in order to explore the rheology of simple mixtures of granular solids and water (Martosudarmo, 1994; Martosudarmo and Johnson, 1997). The unification has been made possible largely by introduction of a new experimental apparatus, a *rolling–sleeve* viscometer (Johnson and Martosudarmo, 1997), for measuring some of the rheological properties of clay, water and medium–grained sand. On the basis of the theoretical model we can use the experimental measurements to determine some of the rheological properties of simple grain–flow materials—mixtures of sand and air or sand and water—and the rheological properties of simple debris—sand, water and clay. With the experimental measurements, the rheological model and appropriate equations of motion we can derive velocity distributions of grain flows and muddy debris flows in channels.

RHEOLOGICAL MODELS

We begin by reviewing the rheological models proposed by several investigators to describe grain flow, debris avalanche, and debris flow.

Bagnold's Original Models for Grain Flows

Bagnold (1954) experimented with neutrally buoyant spherical particles in a coaxial rotating–cylinder device, and distinguished between two limiting cases theoretically, a macro–viscous behavior and a grain–inertia behavior[2]. For the grain–inertia behavior, Bagnold presented a simple theoretical/empirical analysis to explain a normal stress effect, which he termed *dispersive pressure*, and a nonlinear relation between shear stress, σ_{xz}, and velocity gradient, D_{xz}; he ignored the interstitial fluid in deriving an equation for the shear stress. In my terminology, Bagnold's expression for the shear stress is

$$\sigma_{xz} = A\, \rho_s\, sin(\theta)\, (d^3/s)\, F(d/s)\, D_{xz}^2 \qquad (1)$$

in which θ is an angle that depends on the angle of collisions, and d is the diameter, ρ_s is density and s is the spacing between spheres (assumed to be single–sized). Here A and θ are arbitrary (dimensionless) constants and $F(d/s)$ is a function[3], all to be determined experimentally.

Bagnold determined empirically, by curve–fitting, that $F(d/s)$ is roughly equal to (d/s) for spheres spaced so widely that (d/s) is less than 14, but that $F(d/s)$ increases rapidly as (d/s) becomes greater than 14. At a sufficiently large value of (d/s), the spheres lock together. He found that θ varies only slightly with (d/s) and that, for his experiments, $\tan(\theta) = 0.32$ and $a\, \sin(\theta) = 3.9 \times 10^{-3}$ (Bagnold, 1954, p. 58). Thus, based on experimental results with neutrally–buoyant mixtures of spheres and fluid, Bagnold proposed that, for the shear stress,

2 Please note that the purpose of the following discussion is to provide the background, using some new terminology, of a formulation that is somewhat different from Bagnold's, not to show how Bagnold developed his model. I refer to his excellent papers for a proper explanation of his theory.

3 The quantity d/s is a fundamental quantity in Bagnold's analyses. It is an inverse measure of the spacing of particles: d is grain diameter, and s is spacing of particles. Bagnold used the symbol λ for this ratio. Thus, as the spacing becomes large, λ becomes small: as the spacing becomes small, λ can approach infinity. I do not use the linear parameter λ because I want to introduce a volumetric parameter, Θ, that seems to be useful for a wider variety of problems related to debris flow.

$$\sigma_{xz} = \frac{A\rho_s \sin(\theta) d^2}{[\{{}^{s}_{f+s}\Theta_{max}/{}^{s}_{f+s}\Theta\}^{1/3}-1]^2} D_{xz}^{\ 2} \qquad (2a)$$

and, for the "dispersive pressure,"

$$\sigma_{zz} = \frac{A\rho_s \cos(\theta) d^2}{[\{{}^{s}_{f+s}\Theta_{max}/{}^{s}_{f+s}\Theta\}^{1/3}-1]^2} D_{xz}^{\ 2} \qquad (2b)$$

in which the ratio of the grain diameter and the spacing of grains is expressed in terms of concentration, c, that is, so that

$$(d/s) \equiv \lambda \equiv 1/[(c_{max}/c)^{1/3}-1]$$

$$\equiv \frac{1}{[\{{}^{s}_{f+s}\Theta_{max}/{}^{s}_{f+s}\Theta\}^{1/3}-1]} \qquad (2c)$$

in which c_{max} or ${}^{s}_{f+s}\Theta_{max}$ is the maximum possible concentration. The concentration of grains, c,

$$c \equiv V_s/(V_s+V_f) \equiv {}^{s}_{f+s}\Theta \equiv 1/(1+{}^{f}_{s}\Theta) \qquad (2d)$$

is expressed in terms of ratios of volumes[4], Θ, such that the volumetric ratio of fluids to solids is

$${}^{f}_{s}\Theta = volume\ fluid/volume\ solid = V_f/V_s$$

The maximum concentration $c_{max} \equiv {}^{s}_{f+s}\Theta_{max} =$ 0.74 for uniform spheres, and about 0.65 for well–rounded, uniform sand grains (Terzaghi and Peck, 1948; Bagnold, 1954). Some values of volume concentrations of various granular particles are given in Table 1.

Takahashi and Chen Models for Debris Flow and Debris Avalanche

Takahashi (1978, 1991) and Chen (1987, 1988) have largely adopted the equations derived by Bagnold to describe the flow of debris. Takahashi (1991, p. 27), however, differentiates between stresses due to interaction of the granular solids, which he assumes are given by eqs. (2), and stresses due to turbulence in the interstitial fluid (ibid. p. 36–38), which he models as a correction factor to eq. (1),

$$\sigma_{xz} = d^2[A\ \rho_s \sin(\alpha)\ (d/s)^2$$

$$+(\xi s/d)^2\rho_f]\ D_{xz}^{\ 2} \qquad (3a)$$

in which ρ_f is density of the interstitial fluid, $d^2(\xi s/d)^2$ is a mixing length, and ξ is a constant, for which Takahashi suggests a value of 2. Finally, Takahashi (1991) suggests that, for a turbulent debris flow, one adds a third term to eq. (3a),

$$\sigma_{xz} = d^2[A\ \rho_s \sin(\alpha)\ (d/s)^2$$

$$+\ (\xi s/d)^2\rho_f + (l_t/d)^2\rho_d]\ D_{xz}^{\ 2} \qquad (3b)$$

in which ρ_d is the density of the debris and l_t is the mixing length, which is much greater than the mixing length for the interstitial fluid.

4 The widely divergent terminology and notations for volume concentrations of various components that we study for insights into physical properties of debris are hopelessly confused and ambiguous in the literature of soil science, chemistry, pharmacology, geology, ceramics, and geotechnical engineering. Thus, we introduce the universal notation, for example ${}^{s}_{sl+s}\Theta$. Here Θ always means volume ratio, a dimensionless quantity. The leading superscript indicates the quantity in the numerator of the ratio and the leading subscript indicates the quantities in the denominator. In this case, *s* denotes sand and *sl* denotes slurry, so the example indicates the volume ratio of sand to sand plus slurry. Often we use *f* for fluid even if it is a slurry. Furthermore, the notation facilitates the transformation from one system of notation to another. For example, one can express the sand concentration ${}^{s}_{sl+s}\Theta$ in terms of the slurry–to–sand ratio just by inspection of the superscripts and subscripts of the former, dividing each term by the sand volume: ${}^{s}_{sl+s}\Theta = 1/(1+{}^{sl}_{s}\Theta)$. Thus, the notation is both unambiguous and powerful.

McTigue, Savage, Goodman and Cowin Models for Dry Grain Flows

In their research into the flow of dry granular materials, Goodman and Cowin (1971), Cowin (1974, 1978), Savage (1979) and McTigue (1979, 1982) have thoroughly rederived equations for the flow of such materials, starting with the insights provided by Bagnold's analysis of the same problem. Campbell and Brennen (1985) and Campbell (1989) have solved for the flow of dry granular solids in chutes and have performed experiments in order to test the relevance of theoretical models to such flows. Here we will largely follow McTigue (1979, 1982).

Table 1 Volumetric Concentrations

	Densest Packing (c_{max})	Critical State (c_{cs})	Densest Packing (${}^{f}_{s}\Theta_{min}$)	Critical State (${}^{f}_{s}\Theta_{cs}$)
Angular beach sand*	**0.64**	**0.56**	**0.55**	**0.79**
Spherical lead shot*	**0.74**	**0.63**	**0.35**	**0.59**
Ottawa sand	**0.66**	**NA**	**0.52**	**NA**

*(after Bagnold, 1966) Value for densest packing of lead shot is theoretical. Other values measured.

The theoretical ${}^{w}_{s}\Theta_{min}$ value for cubic packing is 0.91, whereas it is 0.35 for tetrahedral packing of perfect spheres. According to the data from Harr (1962), the values of ${}^{w}_{s}\Theta$ are 0.85 for loose packing and 0.52 for dense packing of uniform sand. For the Ottawa sand we used in the study, the value of ${}^{w}_{s}\Theta$ for loosest packing is 0.7, achieved by pouring the sand into a column. The value of ${}^{v}_{s}\Theta$ for densest packing is 0.52, achieved by tapping a sand column.

McTigue (1979, 1982) has re-solved the Bagnold grain-inertia problem, eliminated many of the special assumptions, and generalized his analysis by considering dry granular solids to be similar to a Reiner-Rivlin fluid (Rivlin, 1948; Truesdell and Noll, 1965). According to McTigue and Rivlin, the normal and shear stresses, averaged over an ensemble of grains, are given by, for example,

$$\sigma_{xx} = -p_s + \tau_{mix}\frac{D_{xx}}{\sqrt{-K_2'}} + 4\Lambda_1\sqrt{-K_2'}\left(\frac{1}{{}^{s}_{s+f}\Theta - {}^{s}_{s+f}\Theta_{max}}\right)^2 D_{xx}$$

$$- 4\Lambda_2\left(\frac{1}{{}^{s}_{s+f}\Theta - {}^{s}_{s+f}\Theta_{max}}\right)^2 [(D_{xx}{}^2 + D_{xy}{}^2 + D_{xz}{}^2] \quad (4a)$$

$$\sigma_{xz} = \tau_{mix}\frac{D_{xz}}{\sqrt{-K_2'}} + 4\Lambda_1\sqrt{-K_2'}\left(\frac{1}{{}^{s}_{s+f}\Theta - {}^{s}_{s+f}\Theta_{max}}\right)^2 D_{xz}$$

$$- 4\Lambda_2\left(\frac{1}{{}^{s}_{s+f}\Theta - {}^{s}_{s+f}\Theta_{max}}\right)^2 [(D_{xy}D_{yz} + (D_{xx} + D_{zz})D_{xz}] \quad (4b)$$

$$\tau_{mix} = [C\cos\phi + p_s \sin\phi] \quad (4c)$$

in which the pressure is (Passman and others, 1978)

$$p_s = \alpha({}^{s}_{s+f}\Theta^2 - {}^{s}_{s+f}\Theta^2_{cs}) \quad (4d)$$

Here α is the *pressure coefficient* and Θ_{cs} is the volumetric ratio at the so–called "critical state" of deforming granular materials (McTigue, 1982), some values of which are given in Table 1. In eq. (4c), C is *cohesion* and ϕ is *angle of internal friction* of the granular phase. Λ_1 is the *coefficient of inertial viscosity* and Λ_2 is the *dispersion coefficient*. The invariant is

$$K_2' = (1/2)[D_{ij}'D_{ij}'-D_{ii}'D_{jj}']; \quad D_{ij}' = D_{ij}-D_{kk} \qquad (4e)$$

The quantity $\left(\frac{1}{{}^{s}_{s+f}\Theta-{}^{s}_{s+f}\Theta_{max}}\right)^2$ clearly plays an important role in these equations. The volumetric concentration, ${}^{s}_{s+f}\Theta$ is necessarily less than or equal to the critical concentration. At the critical concentration, the material locks–up and cannot flow; the deformation rate D, goes to zero. Further, for the stress to be finite, the deformation rate must decrease as the volumetric concentration increases and approaches the critical value.

A Model for Macro–viscous and Inertial Flow

Macro–Viscous Flow

In Martosudarmo (1994) and Martosudarmo and Johnson, 1997) we have re–investigated the application of the Coulomb–viscous rheological model to simple debris, consisting of mixtures of water, clay and sand, that was suggested in my early field, experimental and theoretical study of debris flow (Johnson, 1965, 1970). The model is generalized by the simple fluid model developed by Rivlin (1948) and applied by McTigue (1979) in the form of eqs. (4),

$$\sigma_{xx} = -p_s-p_f+\tau_{mix}\frac{D_{xx}}{\sqrt{-K_2'}}+2\eta_{deb}D_{xx}$$

$$-4\Lambda_2\left(\frac{1}{{}^{s}_{s+f}\Theta-{}^{s}_{s+f}\Theta_{max}}\right)^2[D_{xx}{}^2+D_{xy}{}^2+D_{xz}{}^2] \qquad (5a)$$

$$\sigma_{xz} = \tau_{mix}\frac{D_{xz}}{\sqrt{-K_2'}}+2\eta_{deb}D_{xz}$$

$$-4\Lambda_2\left(\frac{1}{{}^{s}_{s+f}\Theta-{}^{s}_{s+f}\Theta_{max}}\right)^2[(D_{xy}D_{yz}$$

$$+(D_{xx}+D_{zz})D_{xz}] \qquad (5b)$$

$$\tau_{mix} = [C\cos\phi+(p_s-p_f)\sin\phi] \qquad (5c)$$

in which p_f is pressure in the fluid phase (generally a mixture of water and clay minerals) and η_{deb} is the viscosity of the debris. The viscosity of the debris seems to be predictable by a remarkably simple expression, derived from mixing theory (Martosudarmo, 1994),

$$\eta_{deb} = \frac{\eta_f}{1-\sqrt[3]{(1+{}^{f}_{s}\Theta_{min})/(1+{}^{f}_{s}\Theta)}} \qquad (5d)$$

Coupling to Migration of Interstitial Fluid

The rheological equations are coupled to the migration of pore fluids for flows with water or slurry in the interstices of the granular phase, as we have shown elsewhere (Martosudarmo and Johnson, 1997). Therefore, we need to couple any solution of a flow problem with a solution to a set of equations for movement of fluids relative the grains. For example, if ψ is the potential of the fluid phase (Bear, 1972),

$$\psi = z\cos(\beta) + x\sin(\beta)+p_f/\gamma_f \qquad (6a)$$

in which x and z are arbitrary Cartesian coordinates, with z tilted at angle β from the direction of gravitational acceleration. If gravity were small compared to other accelerations, eq. (6a) would indicate that the potential is given largely by the fluid pressure. In general, one of the components of flow rate of the fluid phase through the debris is (Bear, 1972)

$$q_x = -{}^fK_{deb}\,\partial\psi/\partial x \qquad (6b)$$

in which ${}^fK_{deb}$ is the hydraulic conductivity of the debris with respect to the fluid phase. Further, the volumetric change in content of the fluid phase with time is given by the continuity equation familiar in groundwater theory (Bear, 1972),

$$\partial {}^f_s\Theta/\partial t = \partial[{}^fK_{deb}(\partial\psi/\partial x)]/\partial x$$

$$+\partial[{}^fK_{deb}(\partial\psi/\partial z)]/\partial z \qquad (6c)$$

For simple debris, containing a single size of coarse grains, the *permeability* is

$${}^f\kappa_{deb} = \frac{(\varphi d)^2}{180}\,\frac{{}^f_s\Theta^3}{1+{}^f_s\Theta} \qquad (6d)$$

in which φ is a shape factor of about 0.61 for well–rounded sand grains (e.g., Bear, 1972). The hydraulic conductivity is

$${}^fK_{deb} = {}^f\kappa_{deb}\,\gamma_f/\eta_f \qquad (6e)$$

These equations indicate that a change in the volumetric concentration of interstitial fluid, ${}^f_s\Theta$, requires a gradient in head, ψ, which generally implies a gradient in pressure, p_f.

We have experimentally determined relations between hydraulic conductivity and volumetric ratios of water to grains, ${}^w_s\Theta$, for the fine-grained Ottawa sand, kaolinite clay and a silt. The values for sand and silt were determined with a fluidizing column, in order to develop the large void ratios (Martosudarmo, 1994). The data are shown as points in Figure 4. The hydraulic conductivity was also calculated using the theory presented by Bear (1972), expressed in eqs. (6d) and (6f), using the average grain size for the sand and silt. The correlation between measurements and theory is excellent except for the low end of the ${}^w_s\Theta$ data for silt. The effective grain size for the clay was simply estimated.

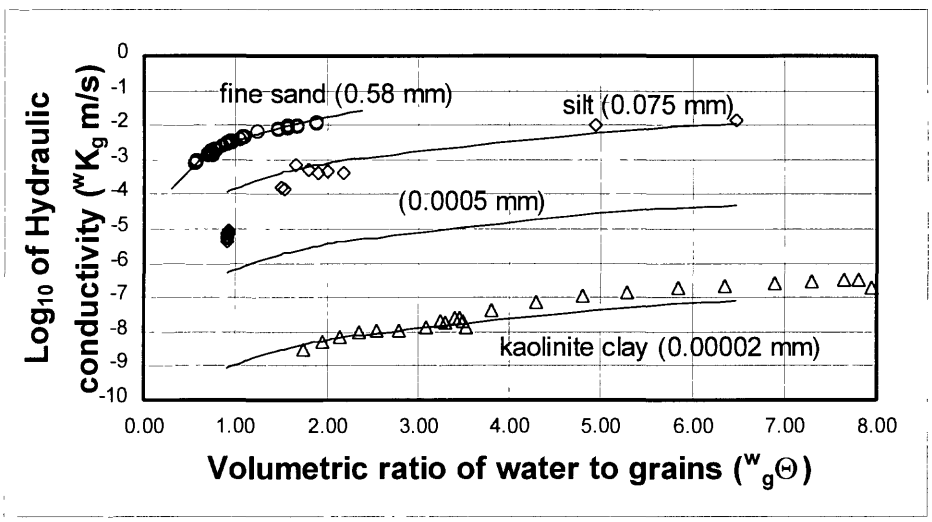

Figure 4. Relations between hydraulic conductivity and volumetric ratio of water to grains. Points are experimental measurements for fine-grained Ottawa sand, silt, and the kaolinite clay used for the rheological experiments described herein. Solid lines are theoretical, according to eqs. (6d) and (6e). Approximate grain sizes indicated in parentheses.

Combined Macro–Viscous and Inertial Flow

To extend the theoretical model from strictly a macro–viscous behavior considered for debris or strictly an inertial behavior considered for dry granular solids, we tentatively propose a more nearly general model, that should closely describe both the macro–viscous and inertial flow of debris. We combine our model for macro–viscous flow, eqs. (5), with McTigue's model for inertial flow, eqs. (4), such that

$$\sigma_{xx} = -p_s - p_f + 2\eta_{deb}\left[1+N_{MB}+\frac{\tau_{mix}}{2\eta_{deb}\sqrt{-K_2'}}\right]D_{xx}$$

$$-4\Lambda_2\left(\frac{1}{{}^{s}_{s+f}\Theta-{}^{s}_{s+f}\Theta_{max}}\right)^2\left[(D_{xx}^2+D_{xy}^2+D_{xz}^2\right] \quad (7a)$$

$$\sigma_{xz} = 2\eta_{deb}\left[1+N_{MB}+\frac{\tau_{mix}}{2\eta_{deb}\sqrt{-K_2'}}\right]D_{xz}$$

$$-4\Lambda_2\left(\frac{1}{{}^{s}_{s+f}\Theta-{}^{s}_{s+f}\Theta_{max}}\right)^2\left[(D_{xy}D_{yz}+(D_{xx}+D_{zz})D_{xz}\right] \quad (7b)$$

in which

$$\tau_{mix} = C\cos\phi+(p_s-p_f)\sin\phi \quad (7c)$$

$$p_s = \alpha({}^{s}_{s+f}\Theta^2-{}^{s}_{s+f}\Theta_{cs}^2) \quad (7d)$$

Here η_{deb} is the viscosity of the mixture, expressed in terms of the viscosity of the fluid phase in eq. (5c). According to Bagnold, for single grain sizes,

$$\Lambda_1 = A\,\rho_s d^2 \quad (7e)$$

where $A = 0.013$ for the spheres and fluids he tested, but Bagnold considered only the inertial behavior in that case. We will leave A or Λ_1 as an empirical constant.

N_{MB} is the *McTigue–Bagnold dimensionless number*

$$N_{MB} = \eta_I/\eta_{deb} \quad (7f)$$

which compares the nonlinear, inertial viscosity, due to grain impact, to the linear, macro viscosity of the mixture. The inertial viscosity is,

$$\eta_I = 2\Lambda_I\left(\frac{1}{{}^{s}_{s+f}\Theta-{}^{s}_{s+f}\Theta_{max}}\right)^2\sqrt{-K_2'} \quad (7g)$$

in which ${}_{s}\Lambda_1$, the *inertial coefficient* (with units of Pa s^2), and ${}_{s+f}\Theta_{max}$ are constants to be determined.

The McTigue-Bagnold number is greater than one if the inertial viscosity is stronger and less than one if it is weaker than the macro–viscous resistance to flow.

The McTigue–Bagnold number derived here is different from the Bagnold number discussed by Takahashi (1991), which was introduced by Bagnold (1954, p. 58) as a number that should allow one to differentiate between flows in which macro–viscous behavior dominates and grain–inertia behavior dominates. Bagnold introduced the dimensionless number,

$$N \cong \frac{\rho_s d^2|D_{xz}|}{\eta_f\sqrt{\sqrt[3]{(1+{}^{s}_{s+f}\Theta_{max})/(1+{}^{s}_{s+f}\Theta)}-1}}$$

as proportional to the ratio of the shear stress according to the grain–inertia theory and the shear stress according to the macro–viscous theory. According to Bagnold (1954), a flow is within the macro–viscous range if $N < 40$ and it is in the grain–inertia range if $N > 450$.

Our McTigue–Bagnold number, eq. (7f), preserves the spirit of Bagnold's dimensionless number, but has the advantage that it is updated based on more recent work and it is greater than one if the nonlinear inertial viscosity is stronger and less than one if the inertial viscosity is weaker than the linear macro–viscosity.

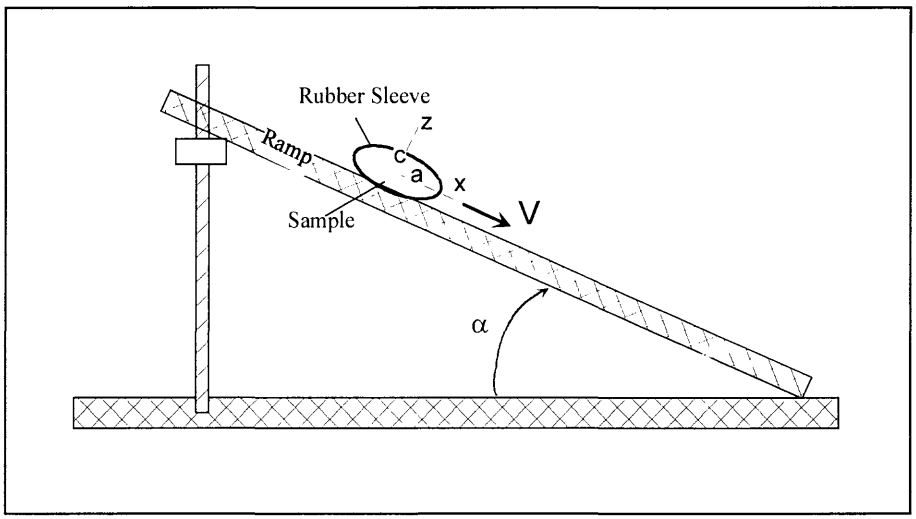

Figure 5. Schematic diagram of rolling–sleeve viscometer. The rubber tube is about 2.5 cm in diameter and 20 cm long; it is closed at each end after the sample is loaded. Its cross section is an oval as it moves down the slope provided by a tilted board, two to three m long. The velocity of the rolling sleeve is measured by determining the time (average of 4 or 5 runs) it takes for the sleeve to move 30 to 40 cm, after terminal velocity is reached.

EXPERIMENTS WITH GRAIN–FLOW AND DEBRIS–FLOW MATERIALS

We have used the rolling sleeve viscometer (Johnson and Martosudarmo, 1997) (Figure 5) to study the *undrained* deformation of classic grain–flow materials, consisting of mixtures of distilled/deionized water and medium–grained sand, and the deformation of simple debris, consisting of mixtures of water, kaolinite clay, and the same medium–grained sand. We have used the same materials so that differences we detect are results of differences we can measure.

Experimental Materials

The medium–grained sand is Ottawa quartz sand[5]. The sand has an average grain size of about 0.6 mm. The grains are well–rounded, nearly spherical. The hydraulic conductivity, K, of the consolidated sand with respect to water ranges from ${}^{w}K_s = 6 \times 10^{-4}$ m/s at a volumetric ratio of water to sand of ${}^{w}_{s}\Theta = 0.52$ to ${}^{w}K_s = 14 \times 10^{-4}$ m/s at ${}^{w}_{s}\Theta = 0.7$. The loosest packing of static Ottawa sand is ${}^{air}_{sand}\Theta = 0.7$. The volumetric ratios of water to dispersed sand ranged from ${}^{w}_{s}\Theta = 0.8$ to ${}^{w}_{s}\Theta = 1.5$ in the experiments.

The slurries used in experiments with simple debris consisted of distilled/deionized water and Georgia kaolinite type SC–25 produced by Akrochem[6]. About 99.7% passes through a 325 mesh and 80% is smaller than 5 microns. The clay has a *plastic limit* (PL) of 33%, or ${}^{w}_{cl}\Theta = 0.85$, and a *liquid limit* (LL) of 63 % or ${}^{w}_{cl}\Theta = 1.63$ (Lambe and Whitman, 1969). The *flow limit* (FL) is about 270 % or ${}^{w}_{cl}\Theta = 7$. The flow limit is defined as the water content at which the slurry can flow freely and the slurry has the ability to erase a streak or a groove formed on its surface, so the surface is always smooth (Tadros, 1987).

5 U.S. Silica Corporation, Ottawa, Illinois 61350 [800–635–7263].

6 Akrochem Corporation, 255 Fountain Street, Akron, Ohio 44304 [800–321–2260].

Properties of Sand–Water (Grain–Flow) Mixtures

Behavior of Deforming Mixtures

When using the rolling–sleeve apparatus, sand and water are sealed in a rubber sleeve, and the sleeve is placed on an inclined ramp (Figure 5; Johnson and Martosudarmo, 1997). If the slope angle of the inclined ramp is low, the sleeve either rolls down the ramp or remains stationary. In general, if the slope is low, and if the rolling sleeve is held onto the surface of the ramp for a few seconds so that the sand can sediment, the sleeve remains stationary when it is released. But if the rolling sleeve is agitated and then quickly released on the ramp, before the sand can sediment, the tube rolls down the slope. If the slope is high enough, the tube rolls down the ramp, picking up speed as the sand dispersed in the fluid, and then maintains constant speed at the terminal velocity. All measurements reported here were made after the rolling–sleeve had achieved terminal velocity. For most mixtures of sand, a few tenths of a meter sufficed for terminal velocity.

We calculate shear stress and deformation rate using the size and shape of the cross section of the rolling sleeve, the mass of the mixture, and the velocity of the rolling sleeve (Johnson and Martosudarmo, 1997):

$$D_{xz} = (V/2c)[1 - (c/a)^2]$$

in which a is the major and c is the minor axis of the ellipse, and V is the down–slope velocity of the center of the ellipse. The shear stress is,

$$\sigma_{xz} = [\pi\, c\, \gamma \sin \alpha]/I$$

where γ is unit weight of debris, α is the slope angle and I is a function of (c/a) in the form of

$$I \approx 4.75\ (1 - c/a), \text{ for } (c/a) \leq 0.5$$

The relations between deformation rate and shear stress for mixtures of sand and water are shown in Figure 5. The actual experimental measurements were velocity of the rolling rubber sleeve, which was used to compute deformation rate, and slope angle of the inclined ramp, which was used to compute shear stress, so one might consider

the plots in Figure 6 to be plots of slope angle on the vertical axis and velocity on the horizontal axis.

Figure 6 shows strings of data points representing the measurements for several different slope angles for each mixture.

Sedimentation in Dispersion Gap

For most mixtures, the high end of the stress/deformation rate relation was determined by convenience but the low end is at minimum deformation rate for which the sample remains dispersed. The low end corresponds to zero deformation rate or else to the minimum deformation rate at which the velocity of the rolling sleeve could be stabilized. The sleeve would slow and might even stop rolling, reflecting sedimentation of the sand for conditions below the low end.

Thus the lower end of each curve relating stress and deformation rate is characterized by a gap, a *dispersion gap*, that is a function of the average shear stress to which the mixture is subjected. For deformation rates within the dispersion gap the mixture will not remain dispersed. For larger deformation rates it will.

The dispersion gap is a function of the average shear stress and the volumetric ratio of water to sand and is defined by the concave–upward, dashed line connecting the ends of the thick lines in Figure 6. The dispersion gap is very small or missing for the mixture with a low volumetric ratio of water to sand, ${}^{w}_{s}\Theta = 0.83$ (Figure 6). For this mixture, the sleeve does not roll unless the shear stress (slope angle) is above a minimum value, corresponding to the static strength of the mixture. But if the slope is above the minimum value, the sleeve rolls as soon as it is placed on the inclined ramp, the sand disperses and the rolling sleeve quickly reaches terminal velocity.

Mixtures with higher volumetric ratios of water display the dispersion gap, but the gap is visible only if the shear stress is sufficiently low. For example, consider the mixture with a volumetric ratio of ${}^{w}_{s}\Theta = 0.9$. First consider large stresses. If a flexible sleeve filled with a mixture of this composition is placed carefully on the inclined ramp, and held to allow time for the sand to settle, different things will happen depending on the shear stress (slope angle). If the slope is high, so the shear stress is high, say 90 Pa (Figure 6), the sleeve, when placed on the inclined ramp, will accelerate and the sand will disperse until the deformation rate in the mixture is about $D_{xz} = 35/s$. The phenomenon is the same for shear stresses as low as 75 Pa, for which the terminal deformation rate was about 23/s. If the sleeve is placed on the ramp and agitated slightly, it accelerates quickly to its terminal value of 23/s. At a shear stress of 67 Pa the dispersion gap is still zero but the envelope of the dispersion gap intersects the stress axis at this shear stress (Figure 6). For a smaller average shear stress of about 55 Pa, the dispersion gap is $D_g = 3/s$. Perturbing deformation rates smaller than this value will lead to sedimentation. The minimum shear stress for this mixture to be dispersed is $\sigma_{min} = 48$ Pa, and the maximum dispersion gap for this mixture is $(D_g)_{max} = 7/s$ (Figure 6).

The dispersion gap becomes visible only for lower slope angles, and corresponding lower shear stresses. The flexible sleeve will not move unless we strongly agitate and remold the sleeve and its contents and then quickly place it on the inclined ramp. For example, for a shear stress of about 55 Pa, a small perturbation in deformation rate is inadequate. Although the flexible sleeve might roll at first, the sand sediments and the sleeve soon stops rolling. With sufficient agitation, though, the rolling of the sleeve becomes unstable and accelerates, the sand disperses, and the sleeve reaches its terminal deformation rate of about 12/s.

Thus, the dispersion gap is a measure of the amount of agitation required to establish steady flow of a mixture. For agitation rates below the dispersion gap, dispersal of the mixture cannot be maintained and the sample sediments. Values of the maximum dispersion gap for various volumetric ratios of water to sand are given in Table 2.

Table 2. Maximum Dispersion Gap of Sand–water Mixtures.

${}^{w}_{s}\Theta$	Maximum Dispersion Gap $(D_g)_{max}$ (1/s)
0.8	0
0.83	1
0.9	7
1.0	26
1.2	40
1.5	59

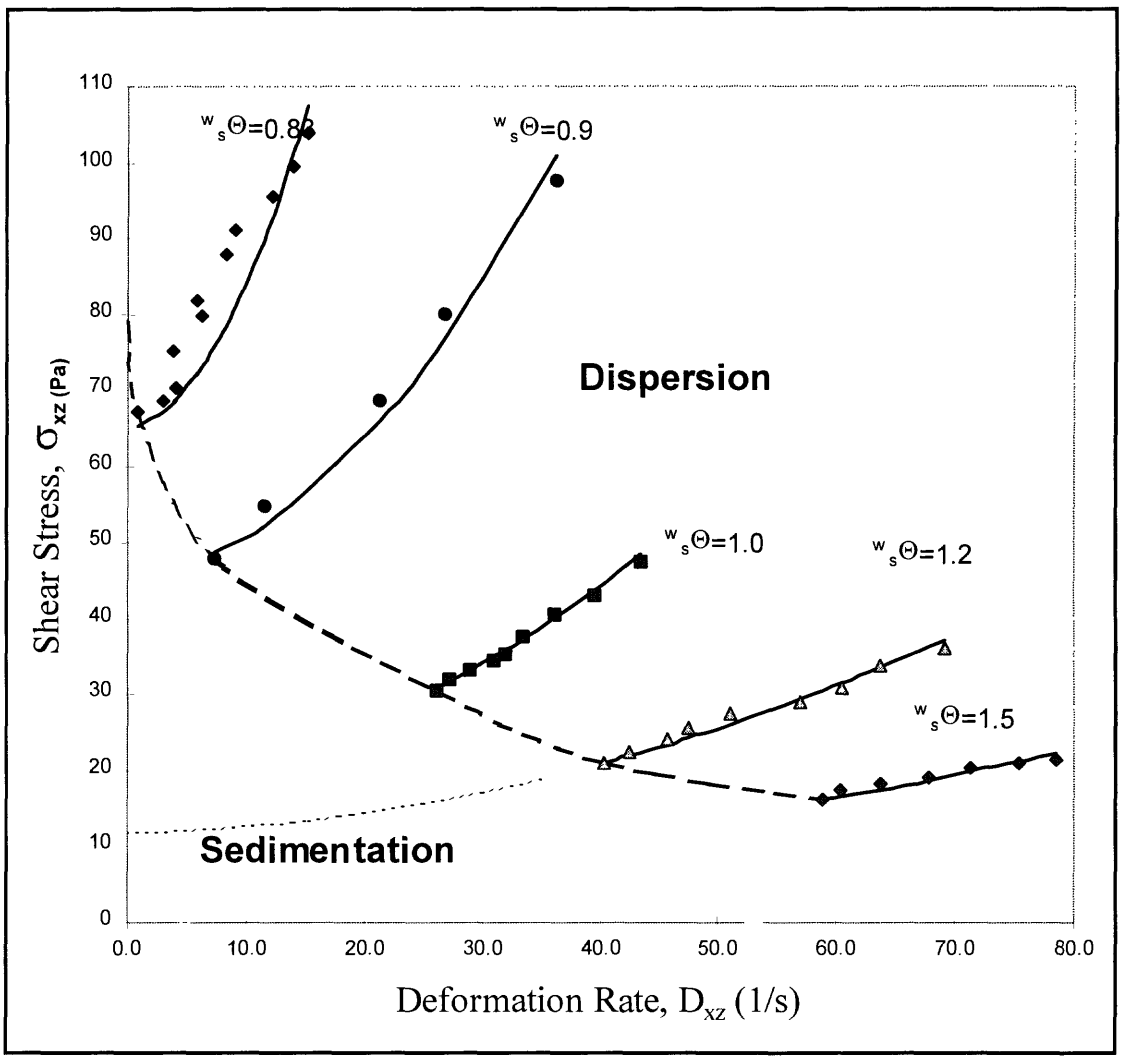

Figure 6. Relations between shear stress applied to debris to deformation rate of debris within rolling sleeve for different volumetric water content, $^{w}_{s}\Theta$, of water to sand. The points are averages of 4 or 5 measurements at each condition. The data for medium–grained sand are represented, roughly, by solid lines, which are based on theory. The lowest datum point for each water content indicates the maximum deformation rate and the minimum shear stress required to maintain uniform flow. For lower deformation rates, the sand sediments and the rolling sleeve slows or stops, so there is a dispersion gap for each mixture. The dashed line connecting the lower ends of the curves is the generalization of the dispersion gap for all mixtures. The dashed line thus marks the boundary between dispersion, above and sedimentation, below. The other heavy dashed line, marked "transition" is boundary between conditions where the macro-viscous resistance of the mixture dominates (to left) and where inertial resistance (banging together of particles) of the mixture dominates (to right).

Matching the Flow Curves

We have drawn the solid lines in Figure 6 on the basis of our model of combined macro–viscous and inertial flow, eqs. (7b) which simplifies to

$$\sigma_{xz} = \tau_B + \frac{2\eta_f}{1-\sqrt[3]{{}^{s}_{w+s}\Theta / {}^{s}_{w+s}\Theta_{max}}} D_{xz}$$

$$+\Lambda_1 \left(\frac{2D_{xz}}{{}^{s}_{w+s}\Theta - {}^{s}_{w+s}\Theta_{max}} \right)^2 \qquad (8a)$$

For mixtures of sand and water, we obtain a critical value of water–to–sand ratio of ${}^{W}_{S}\Theta_{min} \cong 0.77$ (${}^{S}_{W+S}\Theta_{max} = 0.56$) and a value of $\Lambda_1 = 2 \times 10^{-5}$ kg/m by best–fitting the data in Figure 6 with theoretical curves defined by eq. (8a). We have adjusted the constants, Λ_1 and ${}^{W}_{S}\Theta_{min}$ in order to closely fit the data. The third constant, the debris strength, τ_B, translates the curve up or down. For example, the dashed line shown in Figure 6 for a volumetric ratio of ${}^{W}_{S}\Theta = 1.2$ is given by the intercept of the projection of the heavy solid line, along the path of the thin, dashed, curved line, to the stress axis. In this case we see that the strength is about 12 Pa. With our results for the sand–water mixtures we derive an empirical equation for the strength

$$\tau_B \cong \frac{\tau_o}{{}^{W}_{S}\Theta - {}^{W}_{S}\Theta_{min}} \qquad (8b)$$

where $\tau_o \cong 4.5$ Pa. For a volumetric ratio of ${}^{W}_{S}\Theta = 1.2$ we obtain a strength value of 10.9 Pa with eq. (8b). I would emphasize, though, that eq. (8b) is empirical, so the form of the equation and the value of the constant have no physical significance.

Thus we have determined all the constants in eq. (8a) for the sand–water mixtures by means of the rolling–sleeve apparatus.

Comparison with Bagnold's Constants

According to Bagnold's eq. (2a), our constant Λ_1 should be proportional to the density of quartz, to the square of the diameter of the sand grains $(0.00058 \text{ m})^2$ and to a dimensionless coefficient A, which is proportional to a constant and to the sine of an angle. For the sand used in our experiments, we obtain a dimensionless coefficient of $A = 0.025$. The significance of the value for A is quite unclear. Bagnold (1954) estimated a value of $A = 0.013$ for neutrally buoyant spheres in water. Perhaps the factor of two is merely a difference in the formulations.

In order to explore the constants Λ_1 and A, we have experimented with sand and fluids with various viscosities and with plastic beads with a specific gravity similar to that of water (Martosudarmo, 1994). The beads are type P105–212 polymer–bead produced by SoloHill Engineering, Inc[7]. The specific gravity of individual beads is 1.03 to 1.04. The average diameter of the beads is 0.12 mm. The volumetric ratio of voids to beads for loosest packing of the beads is ${}^{air}_{beads}\Theta = 0.65$.

Our results with various mixtures—distilled and deionized water plus beads; salty water and beads (zero density contrast); and water, glycerin and sand—suggest that A could be a function of the grain size and the density contrast of the solid and fluid, but not a function of the viscosity of the fluid or the concentration of the granular phase. The value of A does not depend on the concentration of granular phase for either beads or sand, because the effect of the water–solid ratio is accounted for in the equations, with ${}^{W}_{S}\Theta_{min} = 0.75$ to 0.77 for sand and ${}^{W}_{b}\Theta_{min} = 0.6$ for beads. For Bagnold's experiments with uniform spheres, Figure 7A, ${}^{W}_{S}\Theta_{min} = 0.52$.

The value of A appears to change insignificantly with viscosity of the fluid phase. For mixtures of 5% by weight of glycerin in water, the viscosity of the fluid is $\eta_f = 0.008$ Pa s (about 8 times that of water) and the specific gravity of the fluid is 1.01. For mixtures of 25% glycerin, $\eta_f = 0.032$ Pa s (about 32 times that of water) and the specific gravity is 1.06. Performing a best fit to the data, we determined that $A = 0.03$ for the mixtures with 5% glycerin and $A = 0.04$ for mixtures with 25% glycerin. For pure water, $\eta_f = 0.001$ Pa s and the A-value is 0.025. Thus the A–values appear to change insignificantly with large changes in viscosity.

---

7 SoloHill Engineering, Inc. 1919 Green Rd., Ann Arbor, MI 48105, (313) 665 0453. We found the polymer grains in a scientific supply catalogue. The grains are quite expensive because they have to be carefully prepared for use in various biological experiments, where large, clean surface areas are required. Our use involved relaxed requirements, so we were able to obtain them as rejects from the manufacturer, SoloHill Engineering, at a reasonable cost.

The change in A–value for water–glycerin mixtures may correlate with slight changes in density contrast; as the density contrast decreases, the A–value increases. This is consistent with an increase in A–value from 0.025 for sand–water, with a density contrast of 1650 Kg/m^3, to 0.04 for sand–glycerin–water with a density contrast of 1590 Kg/m^3, to 2 or 4 for bead–water mixtures, with a density contrast of zero to 4 Kg/m^3.

The problem with A as a material constant is that it is constant (A = 0.025) for water and sand at various ${}^{w}_{s}\Theta$ values but it is constant at a very different value, A = 4 for beads and pure water and A = 2 for beads and water containing 6% salt by weight (Sumaryanto and Johnson, 1997).

The parameter that remains constant for bead–water and sand–water mixtures is Λ_1. Thus, for the sand and water, $A = 0.025$, $\rho_s = 2650$ kg/m^2 and $d \cong 0.00058$ m, so that $\Lambda_1 \cong 2 \times 10^{-5}$ kg/m For the beads, $A = 2$ to 4, $\rho_s = 1040$ kg/m^2 and $d \cong 0.00012$ m, so that $\Lambda_1 \cong 3$ to 6×10^{-5} kg/m

The suggestion that Λ_1 is constant is supported by some experiments with silt, for which $A = 1.2$ and $d \cong 0.000075$ m. In this case, $\Lambda_1 = 1.7 \times 10^{-5}$ kg/m. Clearly these values of Λ_1 are nearly constant, and A is not.

Finally, all these values determined with a wide range of experiments are consistent with results of Bagnold's experiments (Figure 7A), from which I obtain a value of $\Lambda_1 = 2.5 \times 10^{-5}$ kg/m. On this basis, I would follow McTigue (1982) in specifying Λ_1 rather than Bagnold's A as a material constant.

Constants Λ_2 and α

Because we do not measure normal stresses with the rolling–sleeve apparatus, we are unable to determine the pressure coefficient, α, or the dispersion coefficient, Λ_2, in the general rheological model, eq. (7a), with the apparatus. Another experiment will have to be designed to measure normal–stress effects. In the absence of such experiments, I will use our rheological equations and Bagnold's experimental results to estimate the dispersion coefficient, Λ_2. Bagnold explained that he had to make several corrections to his experimental data and it appears that in the process, unfortunately, he discarded the information that would have provided us with a way of estimating the pressure coefficient, α.

Figure 7B shows his processed data relating shear stress and normal stress determined experimentally. The solid line is the theoretical curve, assuming a dispersion coefficient, $\Lambda_2 = 7 \times 10^{-5}$ kg/m. There is considerable scatter of the data, though, so values ranging from 2 to 10×10^{-5} kg/m fall within the range of the data shown in the figure.

McTigue–Bagnold Numbers

The relevant form for the McTigue–Bagnold number for sand–water grain–flow materials is given by eq. (7f)

$$N_{MB} = \left(\frac{1}{{}^{s}_{s+f}\Theta - {}^{s}_{s+f}\Theta_{max}}\right)^2 \left(\frac{2\Lambda_1\sqrt{-K_2}}{\eta_{mix}}\right);$$

in which the macro viscosity term in the denominator is derived from mixing theory (Martosudarmo and Johnson, 1997), eq. (5c),

$$\eta_{mix} = \frac{\eta_w}{1-\sqrt[3]{(1+{}^{w}_{s}\Theta_{min})/(1+{}^{w}_{s}\Theta)}}$$

For the conditions of simple shearing in the rolling-sleeve apparatus we can rearrange the equation for the McTigue-Bagnold number and derive a simple relation for the deformation rate in terms of the Bagnold number

$$(dv_x/dz) = \eta_{mix}(N_{MB}/\Lambda_1)\left({}^{s}_{s+f}\Theta - {}^{s}_{s+f}\Theta_{max}\right)^2 \qquad (10a)$$

in which $2\sqrt{-K_2} = (dv_x/dz)$ in eq. (7g)

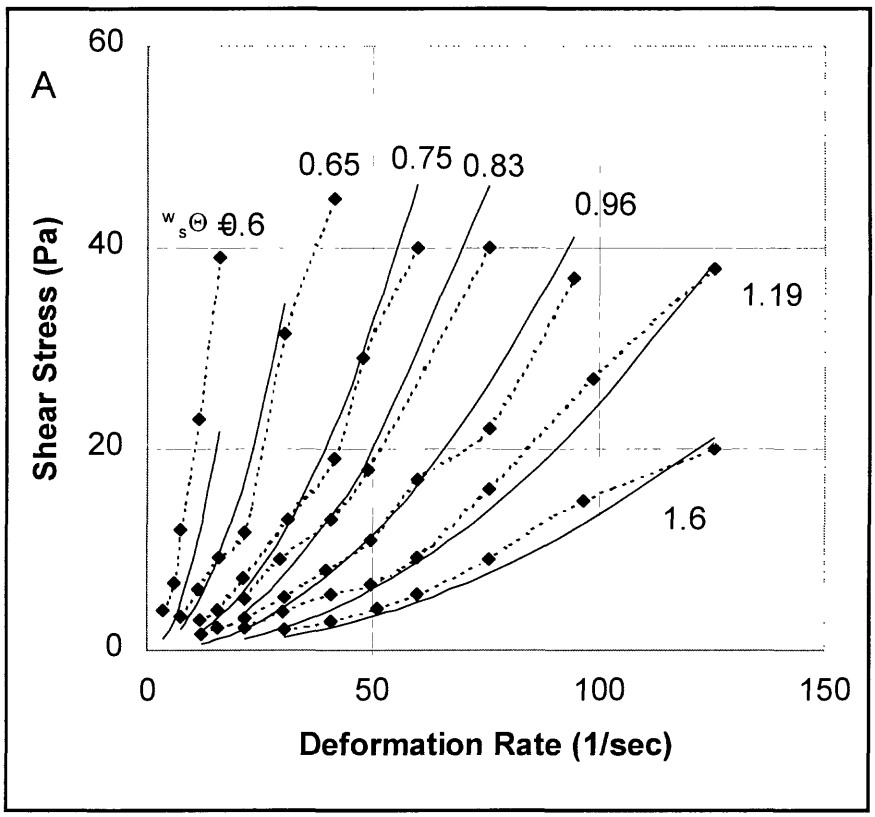

Figure 7. Bagnold's (1954) experimental results for mixtures of neutrally buoyant spheres in a water. A. Relation between shear stress and deformation rate. The numbers next to the curves are the ratios of volumetric ratios of water to spheres, $_{s}\Theta$. B. (Next page)

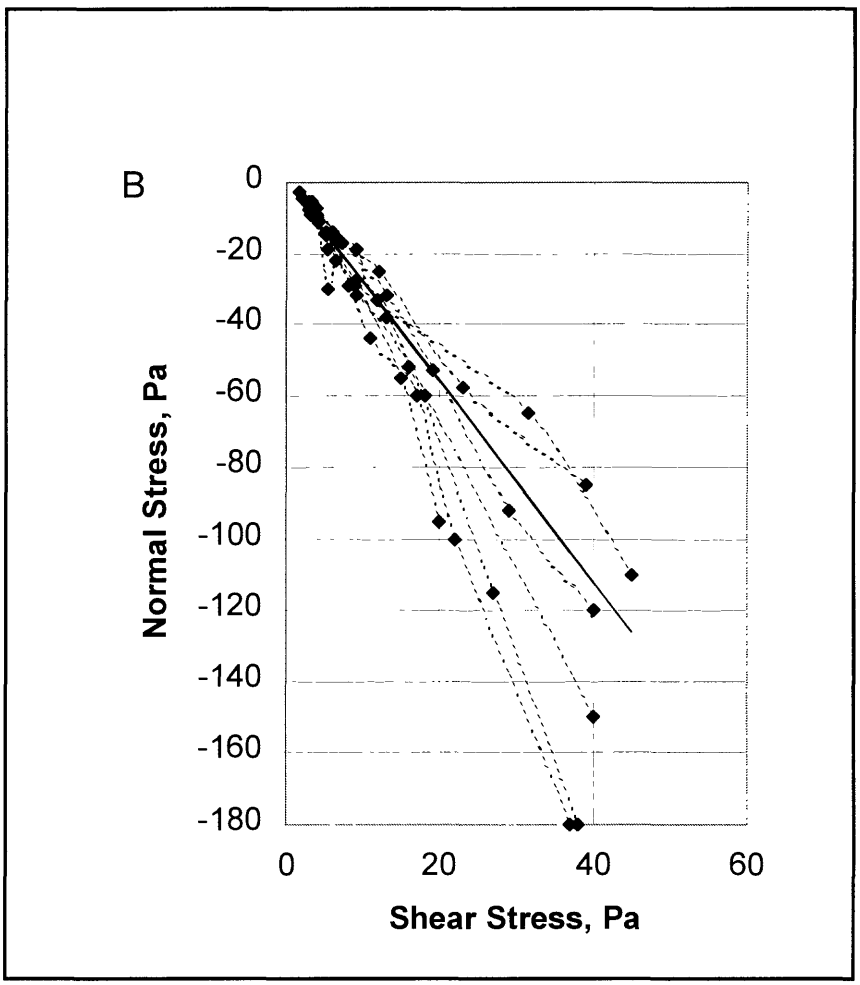

Figure 7B. Relation between normal stress and shear stress for a wide range of mixtures. Each mixture represented by dashed line. Please see Bagnold (1954) for original data.

If we set the McTigue–Bagnold number equal to one in eq. (10a), we can determine the conditions for which the macro–viscous resistance and the inertial terms contribute equally to the resistance to flow. In particular, given all the other variables, we can solve eq. (10) to determine the *transition velocity gradient*, $(dv/dz)_T$, the velocity gradient at which the McTigue–Bagnold number is unity.

$$(dv_x/dz)_T = \eta_{mix}(N_{MB}/\Lambda_l)\left({}^{s}_{s+f}\Theta - {}^{s}_{s+f}\Theta_{max}\right)^2 \quad (10b)$$

Using the appropriate expressions for the parameters in eq. (10b), we have computed the transition velocity gradients[8], $(dv/dz)_T$, presented in the second column in Table 3 as a function of the volumetric ratio of water to sand. The transition velocity gradient ranges from about 0.4/sec to 6.6/sec as the volumetric ratio ranges from 0.8 to 1.5, so the transition velocity gradient is higher for the more dilute mixtures of sand, but it is very small for all mixtures. For velocity gradients higher than transition, the flow is dominated by inertial flow whereas for velocity gradients lower than transition, the flow is dominated by macro–viscous flow. Clearly the sand/water mixtures are dominated by inertial flow.

The domination of the inertial behavior is also reflected in the high average slopes of the flow curves shown in Figure 6. If the points for each ratio of water to sand are fitted with a straight line, we can measure the slopes of the lines and calculate half their values as the *apparent viscosity*. We list the values of apparent viscosity in the third column and the viscosities according to the macro–viscous model in the fourth column in Table 4 as functions of the ratios of water to sand. The viscosities are about an *order of magnitude* larger than those we would predict on the basis of the macro–viscous model, alone, given by the values from mixing theory, in the last column in Table 4. Clearly the flow resistance is largely inertial for the sand–water mixtures.

8 Note that the transition deformation rate, D_T, is simply equal to half the transition deformation rate $(dv/dz)_T$, for the simple flow being considered here.

Properties of Sand–slurry Mixtures (Simple Debris)

We have performed many experiments with mixtures of sand, water and clay and have shown that simple debris has the essential characteristics of debris in muddy debris flows (Johnson, 1965, 1970, 1984; Rodine and Johnson, 1976; Martosudarmo, 1994; Martosudarmo and Johnson, 1997; Johnson and Martosudarmo, 1997). In most of those measurements, we prepared stiff slurries with sufficient strength to support both individual sand particles and groups of sand particles. As a result, the simple debris behaves predominantly as a macro–viscous material. Only if the debris contained large grains would the behavior become inertial. For experiments with mixtures of sand and highly fluid slurry, though, the inertial behaviors become significant.

Reduction of Dispersion Gap

In general, there is no dispersion gap for the mixtures of slurry and sand grains of our experiments. Because the sand particles do not settle, the results are analogous to the experiments with neutrally buoyant beads and water or with sand and highly viscous glycerin solutions. The flow curves extend to, or nearly to, the stress axis.

In one set of experiments with the rolling–sleeve apparatus the simple debris consisted of the same sand used for the grain–flow experiments, but with a dilute clay–water slurry as the fluid. The volumetric ratio of water to clay in the slurry was ${}^{w}_{cl}\Theta = 14$, so the slurry was very dilute; its volumetric ratio of water was twice the flow limit[9] of the clay, so the slurry would be considered to be highly fluid. The dilute slurry is incapable of supporting individual grains of 0.00058 m diameter as well as groups of such grains (Martosudarmo and Johnson, 1997). The coefficient of viscosity of the slurry is 0.015 Pa s (15 times that of water), the strength is 3.3 Pa and the specific gravity is 1.105. The viscosity of the slurry is similar to that of a mixture of water admixed with 15% by weight of glycerin.

9 Defined in section on experimental materials in previous paragraphs.

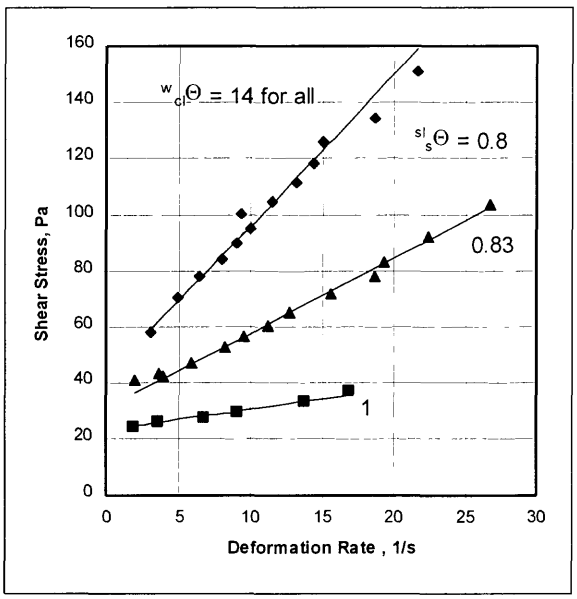

Figure 8. Relations between shear stress and deformation rate of three debris samples with volumetric ratios of slurry to medium-grained sand of $^{sl}_{s}\Theta$ = 0.8, 0.83 and 1.0. The slurry was quite fluid, with a volumetric ratio of water to kaolinite clay of $^{w}_{cl}\Theta$ = 14. For all three debris samples the dispersion gaps are small, less than 3/sec. For sand–water mixtures the dispersion gaps ranged up to 60 /s (Figure 6).

Figure 8 shows flow curves determined with the rolling–sleeve apparatus for volumetric ratios of slurry to sand of $^{sl}_{s}\Theta$ = 0.8, 0.83 and 1.0. For all the flow curves there are dispersion gaps of 2/sec or less, below which the sand grains sediment and above which they disperse. The dispersion gaps for this debris are much lower than those for sand-water mixtures, which range up to about 25/sec for a $^{w}_{s}\Theta$ value of 1.0 (Figure 6). The small dispersion gap for the sand–slurry mixture, as compared to sand–water mixtures, is a result of the low conductivity of the water through the clay slurry and the low conductivity of the slurry through the sand. We have shown elsewhere (Martosudarmo and Johnson, 1997) that sand grains are supported for short times *en masse* by the slurry because the slurry is unable to escape quickly from the pores in the sand. The fluid conductivity of sand with respect to slurry is more than an order of magnitude lower than the hydraulic conductivity of the sand with respect to water.

Bingham Viscosity and Strength of Simple Debris

We have determined the rheological properties of the simple debris as a function of volumetric ratios of slurry to sand and of water to clay. Thus the macro viscosity of simple debris can be derived on the basis of mixing theory (Martosudarmo and Johnson, 1997)

$$\eta_{deb} = \frac{\eta_{slurry}}{1-\sqrt[3]{(1+{}^{sl}_{s}\Theta_{min})/(1+{}^{sl}_{s}\Theta)}} \qquad (11a)$$

where $^{sl}_{s}\Theta$ is the ratio of the volume of slurry to the volume of sand in debris. The critical value of this volumetric ratio, $^{sl}_{s}\Theta_{min}$, for fine-grained Ottawa sand is about 0.77. The value for $^{sl}_{s}\Theta_{min}$ is somewhat larger than the volumetric ratio for loosest packing of dry sand, alone, which is $^{air}_{s}\Theta$ = 0.7. Comparing various values for packing given in Table 1, the critical volumetric ratio we determined for Ottawa sand is only slightly smaller than the volume ratio at the critical state of the sand.

The relation between Bingham viscosity, η_{slurry}, and water content, $^{w}_{cl}\Theta$, of a slurry can be closely calculated with the empirical relation

$$\eta_{slurry} \cong \eta_0 / (^{w}_{cl}\Theta - {}^{w}_{cl}\Theta_{r\eta});$$

$$3.1 < {}^{w}_{cl}\Theta \leq 19. \qquad (11b)$$

using the two arbitrary constants are η_0 = 0.16 Pa s; $^{w}_{cl}\Theta_{r\eta}$ = 3.1. The critical water–clay ratio of 3.1 and the reference viscosity of 0.16 Pa s have no physical significance. Indeed, equation (11b) is invalid for water–clay ratios less than 3.1 and greater than 19, even for the clay used in our experiments.

For the Bingham fluid the friction angle is zero, so the cohesive strength is equal to the Bingham strength, $C = \tau_B$. We have derived an expression for the Bingham strength of debris in terms of the Bingham strength of the slurry, but only empirically. The relation is,

$$(\tau_B)_{debris}/(\tau_B)_{slurry} \approx \frac{C_\tau}{{}^{sl}_{s}\Theta - {}^{sl}_{s}\Theta_\tau};$$

$$0.6 < {}^{sl}_{s}\Theta \leq 5.1 \qquad (11c)$$

where C_τ is an empirical constant and $^{sl}_{s}\Theta_\tau$ is a critical or reference value of slurry–sand ratio.

Table 3. Transition velocity gradients separating macro–viscous and inertial flow regimes for sand–water mixtures.

Volumetric Ratio	Transition Velocity Gradient	Maximum Dispersion Gap of Velocity Gradient
${}^{w}_{s}\Theta$	$(dv_x/dz)_T$ (1/sec)	$[(dv_x/dz)_g]_{max}$ (1/sec)
0.78	1.2	—
0.8	2.4	0
0.83	4.9	2
0.9	8.1	14
1	13.4	52
1.5	19.3	118

* η_f= .001 Pa s. Note: N_{MB} = 1.0 for all

Table 4. Rheological properties of sand–water mixtures.

${}^{w}_{s}\Theta$	Apparent strength (intercept of straight line) τ_B (Pa)	Apparent Viscosity (slope of straight line) η_0 (Pa s)	Macro Viscosity (Mixing Theory) η_{mix} (Pa s)
0.8	74.0	2.2	0.179
0.83	61.6	1.6	0.090
0.9	34.8	0.8	0.043
1.0	5.2	0.5	0.025
1.2	1.0	0.3	0.014
1.5	0.9	0.1	0.009

The straight line that best–fits the data has parameters, C_τ = 3.3 and ${}^{sl}_{s}\Theta_\tau$ = 0.6. The reference value of ${}^{sl}_{s}\Theta_\tau$ = 0.6 is consistent with relatively closely packed grains (Table 1). It is between the loosest and densest packing of the sand in the debris.

The shear strength of the slurry is determined, in turn, with an empirical equation of the same form,

$$(\tau_B)_{slurry} \approx \tau_0/({}^{w}_{cl}\Theta - {}^{w}_{cl}\Theta_\tau);$$

$$3.1 < {}^{w}_{cl}\Theta \leq 19. \qquad (11d)$$

with τ_0 = 35 Pa; ${}^{w}_{cl}\Theta_\tau$ = 3.3. Again, we would emphasize that eqs. (11b), (11c), and (11d) are empirical. Although eq. (11a) is theoretical, it was derived for grains of a single size.

Inertial Viscosity of Simple Debris

We have use the combined macro viscous and inertial model in combination with eqs. (11) to determine the inertial coefficient for the debris, Λ_1. By adjusting the value of Λ_1 and the values of shear strength, we have produced the curves shown in Figure 8 and, on this basis, have selected an inertial coefficient of $\Lambda_1 \cong 10^{-7}$ kg/m. This is much smaller that the value of $\Lambda_1 \cong 2 \times 10^{-5}$ kg/m selected for fluid phases of water or glycerin–water mixtures and solid phases of plastic beads or quartz sand, reported in previous paragraphs. The lower value, however, provides a much better fit to the data; the curves constructed with the larger value are much more curved at ${}^{sl}_{s}\Theta$ values of 0.8 and 0.83 than is suggested by the data for the slurry used in our experiments.

Transition Velocity Gradients

Transition velocity gradients, calculated with eqs. (10) and (11), are consistently very high for the simple debris, so the flow should be macro viscous.

VELOCITY PROFILES FOR CHANNELIZED SAND–WATER GRAIN FLOWS AND SLURRY–SAND DEBRIS FLOWS

Examples of Velocity Profiles

Velocity profiles have been determined in a wide variety of grain–flow and debris-avalanche materials (Takahashi, 1978, 1980, 1987, 1991; Chen, 1985, 1987). For example, Figure 9A shows profiles of velocity, normalized with the maximum velocity at the flow surface, as a function of depth below the surface of grain flows or debris avalanches (called "debris flows") described by Chen (1987). The doubly–curved profile, convex near the surface and concave at depth is perhaps characteristic of such flows. Figure 9B shows a horizontal profile of a debris flow moving in a channel about 2 m wide and the flow was about 1 m deep. The debris is clay-poor, crushed Pelona schist (Rodine and Johnson, 1976) in a 1969 debris flow at Wrightwood, California (Johnson, 1970, 1984). Whereas in Figure 9A we are examining a vertical profile, in Figure 9B we are examining a horizontal profile. The vertical velocity profile in the latter case, though, probably would be roughly equivalent to either half of the profile, with the upper surface corresponding to the centerline of the channel. Thus, we visualize a velocity profile that is quite different, with a distinct *plug* of nondeforming debris near the surface and a profile that is consistently convex throughout the depth, as documented in the first experimental and mechanical analysis of debris flow (Johnson, 1965).

Profiles According to Theoretical Analysis

Governing Equations

We can determine idealized velocity profiles for steady gravity flow of the idealized material down a channel of great width with the constitutive equations and the equilibrium equations. These idealized velocity profiles can then be compared to those of actual flows, shown in Figure 9.

Equilibrium Equations

The relevant equilibrium equations are

$$d\sigma_{zz}/dz = [{}^{s}_{s+f}\Theta\gamma_s + {}^{f}_{s+f}\Theta\gamma_f]\cos(\beta) \qquad (12a)$$

$$d\sigma_{xz}/dz = -[{}^{s}_{s+f}\Theta\gamma_s + {}^{f}_{s+f}\Theta\gamma_f]\sin(\beta) \qquad (12b)$$

in which β is the slope angle of the channel and $[{}^{s}_{s+f}\Theta\gamma_s + {}^{f}_{s+f}\Theta\gamma_f]$ is the unit weight of the debris. γ is the unit weight of a solid or fluid phase.

Rheological Equations

The rheological equations, eqs. (7), simplify markedly for one-dimensional channel flow. Putting the coefficients into dimensionless groups, and rearranging, the equations become,

$${}^{s}_{s+f}\Theta^2 = {}^{s}_{s+f}\Theta^2_{cs}\left(\frac{h\gamma_s}{\alpha}\right)[(\sigma_{zz} + p_f)/h\gamma_s +$$

$$\left(\frac{\Lambda_2}{\Lambda_1}\right)\left(\frac{\sqrt{\Lambda_1/h\gamma_s}(dv_x/dz)}{{}^{s}_{s+f}\Theta - {}^{s}_{s+f}\Theta_{max}}\right)^2] \qquad (12c)$$

$$\left(\frac{\sqrt{\Lambda_1/h\gamma_s}(dv_x/dz)}{{}^{s}_{s+f}\Theta - {}^{s}_{s+f}\Theta_{max}}\right)^2 + \left(\frac{\eta_f}{\sqrt{\Lambda_1 h\gamma_s}}\right)\frac{\sqrt{\Lambda_1/h\gamma_s}(dv_x/dz)}{[1-\sqrt[3]{({}^{s}_{s+f}\Theta)/({}^{s}_{s+f}\Theta_{max})}]}$$

$$= (\sigma_{xz} - \frac{\tau_0}{{}^{w}_{s}\Theta - {}^{w}_{s}\Theta_{min}})/h\gamma_s \qquad (12d)$$

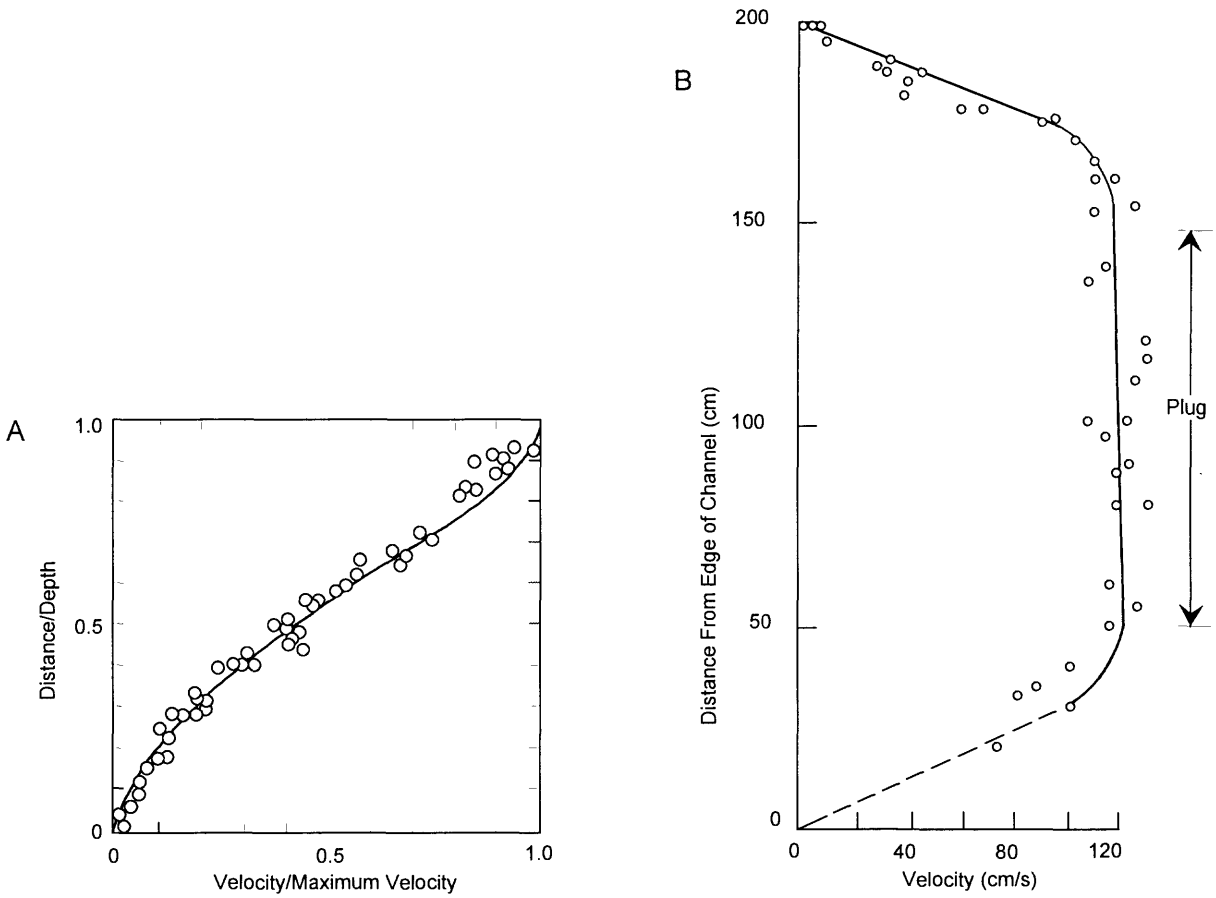

Figure 9. Velocity profiles for a grain flow and a debris flow. A. Vertical velocity profile for some grain flows described by Chen (1987). The top of curve, with maximum velocity, is at top of flow; the bottom, with zero velocity, is at base. The doubly-curved profile—convex near surface and concave near base—is typical of grain flows. B. Horizontal velocity profile of surface of a natural debris flow in a channel at Wrightwood, California. Velocity is zero at edges and maximal in center. The "plug" of uniform velocity in center is typical of muddy debris flows.

in which, for sand–water mixtures, $\tau_0 \cong 4.5$ Pa.

Movement of Pore Fluids

When we add a pore fluid to the flowing granular solid we introduce, of course, many complexities. In order to describe the movement of the pore fluids, we need to couple the rheological and fluid–flow equations. For flow in a wide channel that we are considering here, the volumetric ratio of fluid will change with time and from place to place according to the equation,

$$\partial {}^{f}_{s}\Theta/\partial t = \partial[{}^{f}K_{dcb}(\partial\psi/\partial x)]/\partial x$$

$$+\partial[{}^{f}K_{dcb}(\partial\psi/\partial z)]/\partial z \qquad (12e)$$

The parameters were defined in the vicinity of eq. (6c).

We will consider three special cases of flow in a wide channel in following paragraphs. One relates to a dry granular solid, so that eq. (12e) is of no interest. This problem was solved by McTigue, and we will briefly review it. The others involve a granular solid with a pore fluid, so that eq. (12e) is relevant. We can learn a great deal about the range of behaviors, though, if we consider end members of fluid flow in the pores. These end members correspond, approximately, to pure grain flow or debris avalanche on the one hand and pure muddy debris flow on the other. Clearly there is a continuum, and for the continuum we must address eq. (12e).

In following paragraphs we consider end members because the analyses are simpler, but there are practical reasons as well. As we have shown elsewhere (Martosudarmo and Johnson, 1997), an important element of the behavior of debris flows and debris avalanches is the facility with which the pore fluid can escape from the granular matrix. In the ideal grain flows, there is only water and sand, and the sand has a relatively high hydraulic conductivity (Figure 4). The strong dispersion gap evident in the rolling-sleeve experiments with sand–water mixtures is a result of the relatively high hydraulic conductivity of the pore water with respect to the sand. The insignificant dispersion gap in the case of simple debris with a fluid of slurry is a result of the remarkably, perhaps surprisingly low hydraulic conductivity of the kaolinite clay (Figure 4), essentially locking the water in the clay slurry. Also, it is a result of the inability of the slurry to escape at all or to quickly escape from the pores of the sand as we have documented elsewhere (Martosudarmo and Johnson, 1997).

Thus, for the debris–flow end member we will assume that the conductivities with respect to water and slurry are so low that the fluid cannot escape at all in the time frame of flowage. For the grain–flow end member we will assume that the hydraulic conductivity is so high that the pore–fluid pressures are dissipated immediately.

No doubt there will be interesting conditions between these extremes, but we have postponed analysis of intermediate conditions.

Boundary Conditions

Whatever the rheological properties and the mechanical equations, we must specify appropriate boundary conditions. I have selected the following boundary conditions for the present analysis. The boundary conditions at $z = 0$, that is, at the surface of the flow, are

$$\sigma_{zz} = 0; \quad \sigma_{zz} = 0 \quad p_f = 0$$

For convenience I will assume that the volume fraction of solids is at the critical–state value at the surface of the flow, where the pressure on the solids is zero. Thus, at z = 0 we have that,

$${}^{s}_{s+f}\Theta = {}^{s}_{s+f}\Theta_{cs}$$

At the bottom of the plug, at $z = -z_0$, that is, at the bottom of the plug,

$$\sigma_{xz} = \frac{\tau_o}{{}^{w}_{s}\Theta - {}^{w}_{s}\Theta_{min}};$$

$$\sigma_{zz} = -\alpha({}^{s}_{s+f}\Theta^2 - {}^{s}_{s+f}\Theta^2_{cs}) - p_f\,; \; dv_x/dz = 0$$

At the base of the flow, at $z = -h$, or, where the concentration becomes equal to the critical value, that is, at ${}^{s}_{s+f}\Theta = {}^{s}_{s+f}\Theta_{max}$

$$v_x = 0$$

McTigue Solution

McTigue (1982) has solved the special case of eqs. (12) where the viscosity and unit weight of the fluid phase are zero and the strength is strictly frictional, so that, instead of Bingham strength in eq. (12d) one has the frictional strength,

$$-\alpha \sin(\phi)({}^{s}_{s+f}\Theta^2 - {}^{s}_{s+f}\Theta^2_{cs}) \qquad (13a)$$

Then, by eliminating the square of the deformation rate between eqs. (12c) and (12d), and solving eqs. (12a) and (12c), he derives an expression for the volume fraction of sand as a function of depth, $-z$,

$${}^{s}_{s+f}\Theta = {}^{s}_{s+f}\Theta_{cs} - z/L \qquad (13b)$$

where L *is a characteristic length,*

$$L = \left(\frac{2\alpha}{\gamma_s \cos\beta}\right)\frac{(\Lambda_1/\Lambda_2)-\sin\phi}{(\Lambda_1/\Lambda_2)-\tan\beta} \qquad (13c)$$

The maximum depth of a flow, d_{max}, can be derived from eq. (13b) in terms of the maximum concentration of sand,

$$d_{max} = L({}^{s}_{s+f}\Theta_{max} - {}^{s}_{s+f}\Theta_{cs}) \qquad (13d)$$

McTigue also derives various expressions for the velocity distribution, some of which resemble the convex–concave profiles shown in Figure 9A and some of which resemble the convex profiles shown in Figure 9B, but without the plug. McTigue indicates that, if the characteristic length, eq. (13c) is much larger than the depth of flow, then the concentration is independent of depth, eq. (13b), and the velocity distribution is of the convex form,

$$v_x = v_o[1 - \sqrt{(-z/d)^3}] \qquad (13e)$$

where v_0 is the velocity at the upper surface. For other shapes of velocity profiles, the reader is referred to McTigue's (1982) paper.

Undrained Flow

Muddy debris flows tend to flow in channels under undrained conditions because of the inability of the slurry to escape quickly from the pores of the granular phase and because of the frequent mixing of debris at the front of the flow and where the debris moves over irregularities in the channel bottom (Johnson, 1970).. In these flows the pore-fluid pressures will be high; they will be supporting much of the load of the sediment.

In terms of the theory, we would characterize undrained flow with eq. (12c), such that

$${}^{s}_{s+f}\Theta^2 - {}^{s}_{s+f}\Theta^2_{cs} = 0$$

$$\sigma_{zz} + p_f + \Lambda_2\left(\frac{dv_x/dz}{{}^{s}_{s+f}\Theta - {}^{s}_{s+f}\Theta_{max}}\right)^2 = 0 \qquad (14a)$$

That is, the pore–fluid pressure adjusts itself so that it cancels the overburden pressure and the dispersive pressure, and the concentration of grains remains at the critical state throughout the flow.

The condition of undrained flow considerably simplifies the solution of the differential equations because we can immediately solve the equilibrium equations, eqs. (12a), (12b),

$$\sigma_{zz} = [{}^{s}_{s+f}\Theta\gamma_s + (1 - {}^{s}_{s+f}\Theta)\gamma_f]z\cos(\beta)$$

$$= \gamma_{deb}\, z\cos(\beta) \qquad (14b)$$

$$\sigma_{xz} = -[{}^{s}_{s+f}\Theta\gamma_s + (1 - {}^{s}_{s+f}\Theta)\gamma_f]z\sin(\beta)$$

$$= -\gamma_{deb}\, z\sin(\beta) \qquad (14c)$$

The remaining flow equation, eq. (12d), becomes, in dimensionless form

$$(dv_x^*/dz^*)^2 + \eta_{mix}^* (dv_x^*/dz^*) + [z^* \sin(\beta) + \tau_B^*] = 0 \qquad (14d)$$

in which the dimensionless variables are

$$\tau_B^* = \frac{\tau_B}{h\,\gamma_{deb}}$$

$$\eta_{mix}^* = \eta_f \frac{{}^{s}_{s+f}\Theta_{max} - {}^{s}_{s+f}\Theta}{\sqrt{\Lambda_1 h \gamma_{deb}}\left(1 - \sqrt[3]{{}^{s}_{s+f}\Theta / {}^{s}_{s+f}\Theta_{max}}\right)};$$

$$v_x^* = \frac{v_x \sqrt{\Lambda_1 / h^3 \gamma_{deb}}}{({}^{s}_{s+f}\Theta_{max} - {}^{s}_{s+f}\Theta)}$$

$$z^* = z/h \qquad (14e)$$

The thickness of the plug, the region that is not shearing, is obtained by setting the last term in brackets in eq. (14d) equal to zero,

$$h_{plug} = \tau_B / \gamma_{deb} \sin(\beta) \qquad (15a)$$

and the velocity distribution for the flowing debris below the plug is obtained by solving and integrating eq. (14d),

$$v_x = -\left(\frac{\eta_{mix}^*}{2}\right)(1+z^*)$$

$$-[2/3\sin(\beta)]/\sqrt{((\eta_{mix}^*/2)^2 - \tau_B^* + \sin(\beta))^3}$$

$$-\sqrt{((\eta_{mix}^*/2\Lambda_1)^2 - \tau_B^* - z^* \sin(\beta))^3}] \qquad (15b)$$

Although the expression for the velocity distribution in eq. (15b) for undrained flow of debris is more complex than the special case derived by McTigue for the flow of dry grains, eq. (13e), the distributions are of the same form. The velocity profile consists of a plug and a convex velocity profile below the plug.

The idealization of the undrained flow of debris should closely describe the velocity profile in the vicinity of the snout of a debris flow, where the debris moves much as in the rubber sleeves in our experiments and much as a caterpillar tread. As a debris flow moves along, dilated debris near the surface of the flow in the snout region is quickly turned over to become the debris in the shear zone near the base of the flow. If the conductivity of the debris with respect to the fluid phase is low, the debris near the base should remain dilated and therefore quite fluid. As the snout travels far down the channel, though, the debris left near the base will contract or expand, as the fluid phase is expelled or sucked inward, depending on the normal stress and on the velocity gradient. The velocity distribution, therefore, can be quite different far back from the snout as compared to the snout region of a debris flow.

Figure 10A shows the velocity profile, determined by eq. (15b), with the parameters measured for simple debris, consisting of dilute slurry and sand. The parameters for the solution are: $\beta = 10°$, h = 0.1 m, ${}^{s}_{s+sl}\Theta_{cs} = 0.79$ and ${}^{w}_{cl}\Theta = 14$. The properties are as determined experimentally and described in previous pages. The maximum velocity for these conditions is 4.9 m/s. The profile has the classic shape (Johnson, 1965, 1970) for debris flows, with a prominent plug above and a roughly parabolic profile below. Putting the mirror image of this profile on top of the profile shown in Figure 10A, we obtain the kind of surface profile of the debris flow shown in Figure 9B.

Figure 10B shows the velocity profile according to parameters determined experimentally for sand and water, grain–flow materials. The parameters for the solution were the same as those for the simple debris except, of course, the volumetric ratio of water to clay. The maximum velocity for the grain flow is 6.9 m/s. The profile has the same shape as that determined by McTigue (1982) for dry grain flows, as expressed in eq. (13e).

It is important to realize, though, that we are making a serious (weak) assumption in deriving eqs. (14) and in determining the velocity distribution for a grain flow. We are assuming that, somehow, the flow is undrained. This is a reasonable conclusion for the muddy debris flow, but definitely not for the grain flow. The grain flow would drain quickly so that the excessive pore-water pressures would dissipate, and the flow might stop. The typical

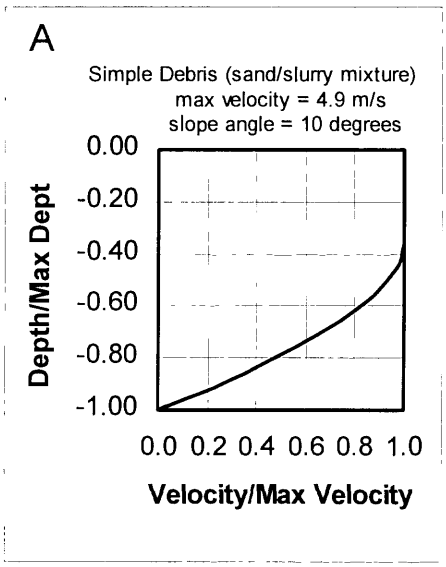

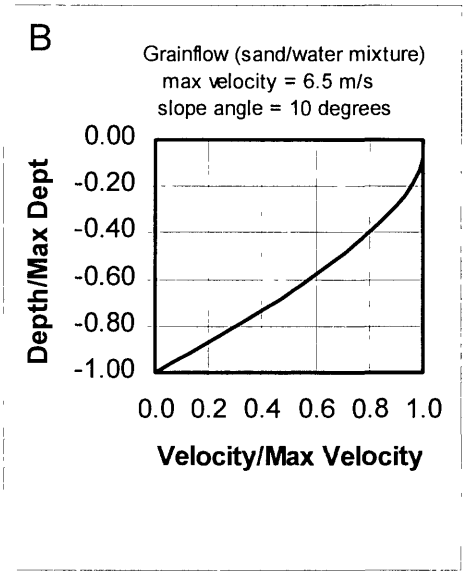

Figure 10. Theoretical vertical velocity profiles according to theory of grain flow and debris flow, assuming undrained conditions. A. Velocity profile for simple debris with dilute slurry in matrix of fine-grained sand, according to theory and properties measured for the simple debris and slurry. The volumetric water content of the slurry was ${}^{w}_{cl}\Theta = 14$ and the sand content of the debris was ${}^{s}_{s+sl}\Theta = 0.79$. The slope angle of the wide channel was taken to be 10° and the depth of the flow was taken to be 0.1 m. The maximum velocity for these conditions is 4.9 m/sec. The profile has the classic shape for muddy debris flows, with a prominent plug and a parabolic profile below the plug. B. Velocity profile for grain-flow material. The volumetric content of sand was the same, ${}^{s}_{s+w}\Theta = 0.79$. The maximum velocity for the grain flow was 6.9 m/sec. The profile has the same shape as that of the simple debris flow, except the plug is much less prominent. As indicated in the text, though, the assumption of undrained flow for such a grain flow is inappropriate, so this profile is largely irrelevant to grain flow.

debris flow would remain undrained, at least in its snout region, and would flow there much as described in Figure 10A.

These conclusions are supported by calculations and measurements of conductivity of simple debris with respect to water and conductivity of sand with respect to slurry. The conductivity of slurry with respect to sand, induced by settling of the sand, is negligible for slurry with volumetric ratios of water to clay of ${}^{w}_{cl}\Theta = 14$ and volumetric ratios of slurry to sand of even ${}^{sl}_{s}\Theta = 5$, let alone ${}^{sl}_{s}\Theta = 0.78$ as assumed here (fig. 5.6, Martosudarmo, 1994).

The conductivity of debris with respect to water would be on the order of ${}^{w}K_{deb} = 10^{-6}$ m/s (ibid.). In contrast, the conductivity of water through sand at the same fluid to solid ratio (${}^{w}_{s}\Theta = 0.78$) is about ${}^{w}K_{s} = 10^{-3}$ m/s (ibid., Figure 4). This is three orders of magnitude higher than the conductivity of water through the sand containing dilute clay–water slurry.

The drastic difference in conductivity of the grain–flow material and the debris–flow material explains not only the large dispersion gap in grain flow and the minor dispersion gap in debris flow, but it also explains the ability to maintain debris flow and the inability to maintain grain flow on low slopes.

Completely Drained Flow

In general, we cannot assume undrained conditions of the fluid phase of clay and water in debris flows and grain flows so that we must account for differences of concentrations of grains within a flow and for movement of the fluid phase. In order to describe the movement of the fluid phase and the pressure in the fluid phase, we must couple the interstitial fluid flow equation, eqs. (6), with the rheological and equilibrium equations, eqs. (12). This makes the problem a transient, time–dependent problem.

There is, however, a second interesting but less complicated case of debris flow or grain flow where the fluid phase has completely equilibrated, so that there is no excess or deficit of pressure in the fluid phase. We would expect this case to be relevant to most flows in which the conductivity of the debris with respect the fluid phase, ${}^{f}K_{deb}$, (eq. 6a), is very high, such as water moving through sand. Also, we would expect it to apply satisfactorily to conditions even in some debris flows, but only well back from the snout of a debris flow moving down a long channel. Near the snout and in channels where there are periodic waterfalls that mix the debris, the flow conditions are probably best described with the model for undrained flow, described above. If, however, the debris has been shearing long enough, without turning over, the excess pressure in the fluid phase should dissipate and the undrained condition should pertain. In such cases, the pressure within the fluid phase is strictly hydrostatic, and

$$dp_f/dz = -\gamma_f \cos(\beta)$$

A Numerical Method

Even for the steady state, though, the general governing equations for the macro–viscous, inertial material, eqs. (12), are highly nonlinear. Fortunately we can use the following strategy to produce a solution. We work from the surface downward to obtain a solution for the velocity gradient, the stresses and the concentrations. Then we work from the bottom upward to obtain the velocities. It is convenient to transform the equilibrium equations, eqs. (12a) and (12b), such that we can integrate eqs. (12a) and (12b) directly,

$$d\sigma_{zz}/d\zeta = \gamma_s \cos(\beta); \quad d\sigma_{xz}/d\zeta = -\gamma_s \sin(\beta)$$

$$\sigma_{zz} = \zeta \gamma_s \cos(\beta) \qquad (16a)$$

$$\sigma_{xz} = -\zeta \gamma_s \sin(\beta) \qquad (16b)$$

where

$$d\zeta = \{{}^{s}_{s+f}\Theta + (1-{}^{s}_{s+f}\Theta)(\gamma_f/\gamma_s)\}\, dz \qquad (16c)$$

is a transformed coordinate in the direction normal to the surface of the flow. We cannot, however, directly integrate the equation for the pressure in the interstitial fluid, rather we must solve the equation

$$dp_f/d\zeta = -[\gamma_f/\{{}^{s}_{s+f}\Theta + {}^{f}_{s+f}\Theta(\gamma_f/\gamma_s)\}]\cos(\beta) \qquad (16d)$$

which is coupled to the other equations that involve the concentration distribution.

Substituting the transformed coordinates into eqs. (12c) and (12d), using eqs. (12f), (16a) and

(16b), and putting the equations in dimensionless form,

$$ {}^{s}_{s+f}\Theta^{2} = {}^{s}_{s+f}\Theta^{2}_{cs} - \left(\frac{1}{\alpha^{*}}\right)[\zeta^{*}\cos(\beta) $$

$$ +p^{*}_{f} + \Lambda^{*}\left(\frac{\{{}^{s}_{s+f}\Theta+(1-{}^{s}_{s+f}\Theta)\gamma^{*}\}(dv^{*}_{x}/d\zeta^{*})}{{}^{s}_{s+f}\Theta-{}^{s}_{s+f}\Theta_{max}}\right)^{2}] \qquad (16e) $$

$$ \left(\frac{\{{}^{s}_{s+f}\Theta+(1-{}^{s}_{s+f}\Theta)\gamma^{*}\}(dv^{*}_{x}/d\zeta^{*})}{{}^{s}_{s+f}\Theta-{}^{s}_{s+f}\Theta_{max}}\right)^{2} $$

$$ + eq\ \frac{\eta^{*}_{f}[{}^{s}_{s+f}\Theta+(1-{}^{s}_{s+f}\Theta)\gamma^{*}](dv^{*}_{x}/d\zeta^{*})}{[1-\sqrt[3]{({}^{s}_{s+f}\Theta)/({}^{s}_{s+f}\Theta_{max})}]} $$

$$ = -[\zeta^{*}\sin(\beta) + \frac{\tau^{*}_{o}}{{}^{w}_{s}\Theta-{}^{w}_{s}\Theta_{min}}] \qquad (16f) $$

The dimensionless variables are chosen to expose the variables and subdue the constants,

$$ \alpha^{*} = \frac{\alpha}{h\gamma_{s}} $$

$$ \tau^{*}_{o} = \frac{\tau_{o}}{h\gamma_{s}} $$

$$ \eta^{*}_{f} = \frac{\eta_{f}}{\sqrt{\Lambda_{1}h\gamma_{s}}} $$

$$ \gamma^{*} = (\gamma_{f}/\gamma_{s}) $$

$$ v^{*}_{x} = v_{x}\sqrt{\Lambda_{1}/h^{3}\gamma_{s}}\ ;\ \zeta^{*} = \zeta/h;\ \Lambda^{*} = \frac{\Lambda_{2}}{\Lambda_{1}} \qquad (16g) $$

In solving these equations, we assume the conditions at the upper surface mentioned in connection with eqs. (12), including that the concentration, ${}^{s}_{s+f}\Theta$, is at the critical state value, ${}^{s}_{s+f}\Theta_{cs}$, and that the velocity gradient is zero. Then, during the first iteration, we assume that the concentration remains at the critical state value for a small incremental distance, ζ, below the surface. During this iteration, we solve eq. (16d) for the fluid pressure, then eq. (16f) for the velocity gradient, $dv_x/d\zeta$, and eq. (16e) for the concentration, ${}^{s}_{s+f}\Theta$. The velocity gradient is zero unless the shear stress exceeds the shear strength, which, itself, is a function of the concentration. This ends the first iteration.

(Figure on next page)

Figure 11. Theoretical velocity profiles for sand–water, grain–flow materials, using material properties determined experimentally for sand–water mixtures. In all three runs we use the dimensionless dispersion coefficient computed using Bagnold's data for the dispersion coefficient and our data for the macro viscosity. Normalized theoretical velocity profiles. Thickness of flow 0.1 m. Thick curve is velocity profile. Thin curve is volumetric ratio of fluid to solid, ${}^{w}_{s}\Theta$, which begins at the critical–state value at the surface. Dimensionless dispersion coefficient of $\Lambda^{*} = 2.8$. The parameter α is unknown, so two different values of the dimensionless variable, α^{*}, are assumed for the runs. In the first two runs, A and B, the difference is the slope angle and $\alpha^{*} = 10$. A. The slope angle is 8°. The depth of the flow is equal to the maximum depth so that the entire thickness of material is flowing, except for a small plug at the surface of the flow. The velocity profile has the convex shape that we saw in undrained flow. The flow is sufficiently intense for the mixture to remain dispersed at depth. The maximum velocity is very large, about 20 m/sec. B. The slope angle is 4°. The depth of flow is greater than the maximum depth so that the lower part of the debris cannot flow—it produces a sediment plug. The sediment plug is a result of the inability of the mixture to remain dispersed at depth, so the sand sediments there. The shape of the velocity profile is convex in the upper part and concave in the lower part, above the sediment plug, as is characteristic of dry flows. C. In this run the dimensionless variable, $\alpha^{*} = 1$, is reduced by an order of magnitude, while keeping the dispersion coefficient high, to explore the effect of the former on the velocity profile. As a result of the low pressure coefficient, the volumetric concentration of fluid decreases from the critical state to a maximum concentration at about middepth. There is an obvious nondeforming plug in this part of the flow. Below middepth, the volumetric concentration of fluid increases because of the high dispersion coefficient, and the higher shear stress there, so the lower part of the flow becomes a zone of high shearing.

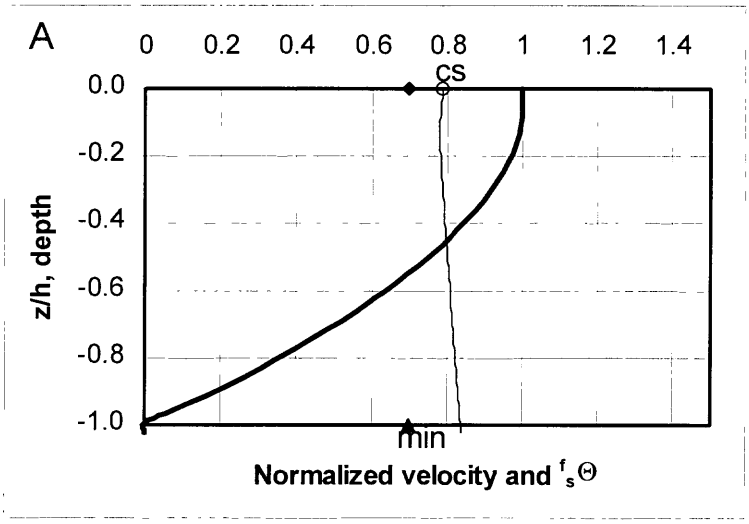
A
0
0.2
0.4
0.6
0.8
1
1.2
1.4
cs
0.0
-0.2
-0.4
-0.6
-0.8
-1.0
z/h, depth
min
Normalized velocity and $f_s\Theta$

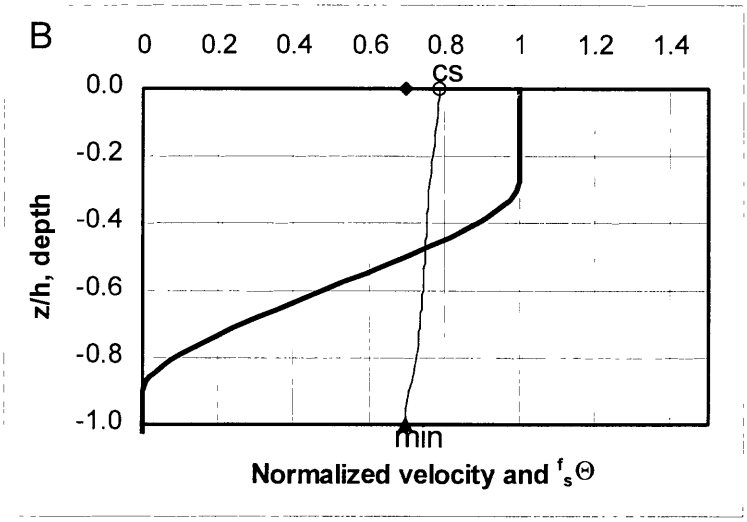
B
0
0.2
0.4
0.6
0.8
1
1.2
1.4
cs
0.0
-0.2
-0.4
-0.6
-0.8
-1.0
z/h, depth
min
Normalized velocity and $f_s\Theta$

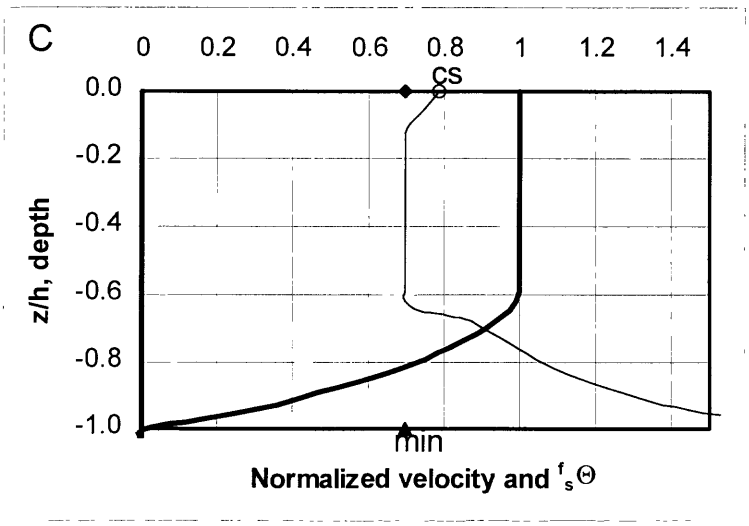
C
0
0.2
0.4
0.6
0.8
1
1.2
1.4
cs
0.0
-0.2
-0.4
-0.6
-0.8
-1.0
z/h, depth
min
Normalized velocity and $f_s\Theta$

Using the new estimate of the concentration, we repeat the procedure described above for eqs. (16d), (16e) and (16f), obtaining an improved estimate of the fluid pressure, the velocity gradient and the concentration at the same depth, ζ. We iterate the solution six times and then numerically integrate to compute the distances, z, corresponding to the distances, ζ.

Finally, we numerically integrate the velocity gradient from the base of the flow where the velocity is zero upwards to the free surface of the flow, using Newton–Cotes quadrature (Milne, 1949, p. 122).

Grain Flow

Figure 11 shows theoretical velocity profiles for sand–water mixtures. The mixtures have the properties determined experimentally with the rolling–sleeve apparatus, so that some of the dimensionless parameters are $\eta^* = 0.004$; $\tau^*_o = 0.001$. To obtain a solution, we must assume two other parameters, Λ_2 and α. For Figure 11A and Figure 11B we assume that the dimensionless dispersion coefficient $\Lambda^* = 2.8$ and the dimensionless pressure coefficient $\alpha^* = 10$. The dimensionless dispersion number is based on measurements made by Bagnold (1954). The dimensionless pressure coefficient is merely selected. Bagnold's measurements provide no guidance.

Figure 11A shows a velocity profile for a sand–water grain flow with a thickness of $h = 0.1$ m flowing down a slope inclined at an angle of 8°. At this slope angle, the maximum depth is equal the actual depth, so the entire thickness of sand–water mixture is flowing, except for a small *strength plug*, about 0.08 h thick, at the top of the profile. The strength plug is generally missing from analyses of grain flows and dry flows (e.g., Takahashi, 1991). It is a result of the strength of the debris and it plays an important role in muddy debris flow (Johnson, 1965, 1970). The velocity distribution has the characteristic, convex shape that we obtained from the solution for undrained flow. Indeed, the distribution of volumetric ratios of fluid to solid, shown with the thin line, indicates that the volumetric ratio starts at the critical state value of ${}^{w}_{s}\Theta = 0.79$ at the top, decreases slightly with depth and then reverses and increases slightly to a value of about 0.83 at the bottom. Thus the flow is sufficiently intense for the sand to remain dispersed at depth. The maximum velocity is very high, however, about 20 m/s, so the flow probably is too rapid for laminar flow to pertain.

Figure 11B shows the same mixture, with the same properties, flowing down a channel with a shallower slope, in this case $\beta = 4°$. The maximum velocity is an order of magnitude smaller. The distribution of velocity is quite different from the flow on the higher slope (Figure 11A) in two respects. The first difference is that the profile has convex upper and concave lower shapes that are characteristic of flow of dry granular solids or granular solids and water (e.g., Figure 9A; McTigue, 1979; Takahashi, 1991). The strength plug at the top is a more prominent feature of the flow on the lower slope. Within the upper part, the velocity decreases nearly linearly with distance below the strength plug and becomes zero at a depth of about 0.75 h where the sand locks up.

The second difference is the occurrence of a *sediment plug* in the lower part of the flow. The sediment plug is quite different from the strength plug. A sediment plug forms if lower part of the material is unable to flow because the mixture has consolidated to the extent that the mixture locks. The formation of the sediment plug is closely related to the dispersion gap that we described in connection with the experiments with the rolling sleeve. They both are a result of sedimentation.

For the example being studied in Figure 11B, the deformation rate (shear stress) is inadequate to disperse the sand at depth as a result of the combination of a dispersion coefficient of $\Lambda^* = 2.8$ and a pressure coefficient of $\alpha^* = 10$. For these conditions, the volumetric ratio of water to sand ${}^{w}_{s}\Theta$ increases downward from the critical state value at the top to the minimum concentration at a depth of 0.85 h. The sand sediments and locks up at depth below 0.85 h while the mixture in the upper part continues to flow.

Thus, there is a minimum slope angle for flow of the mixture 0.1 m thick in a channel without a sediment plug forming. This minimum slope angle is closely related to the maximum deformation rate that we have termed the dispersion gap. For the particular mixture studied here, and for the assumed dispersion coefficient $\Lambda^* = 2.8$ and $\alpha^* = 10$, the minimum slope angle is 4.3°.

In comparing Figure 11A and Figure 11B we note that the shearing rate is sufficient at the higher

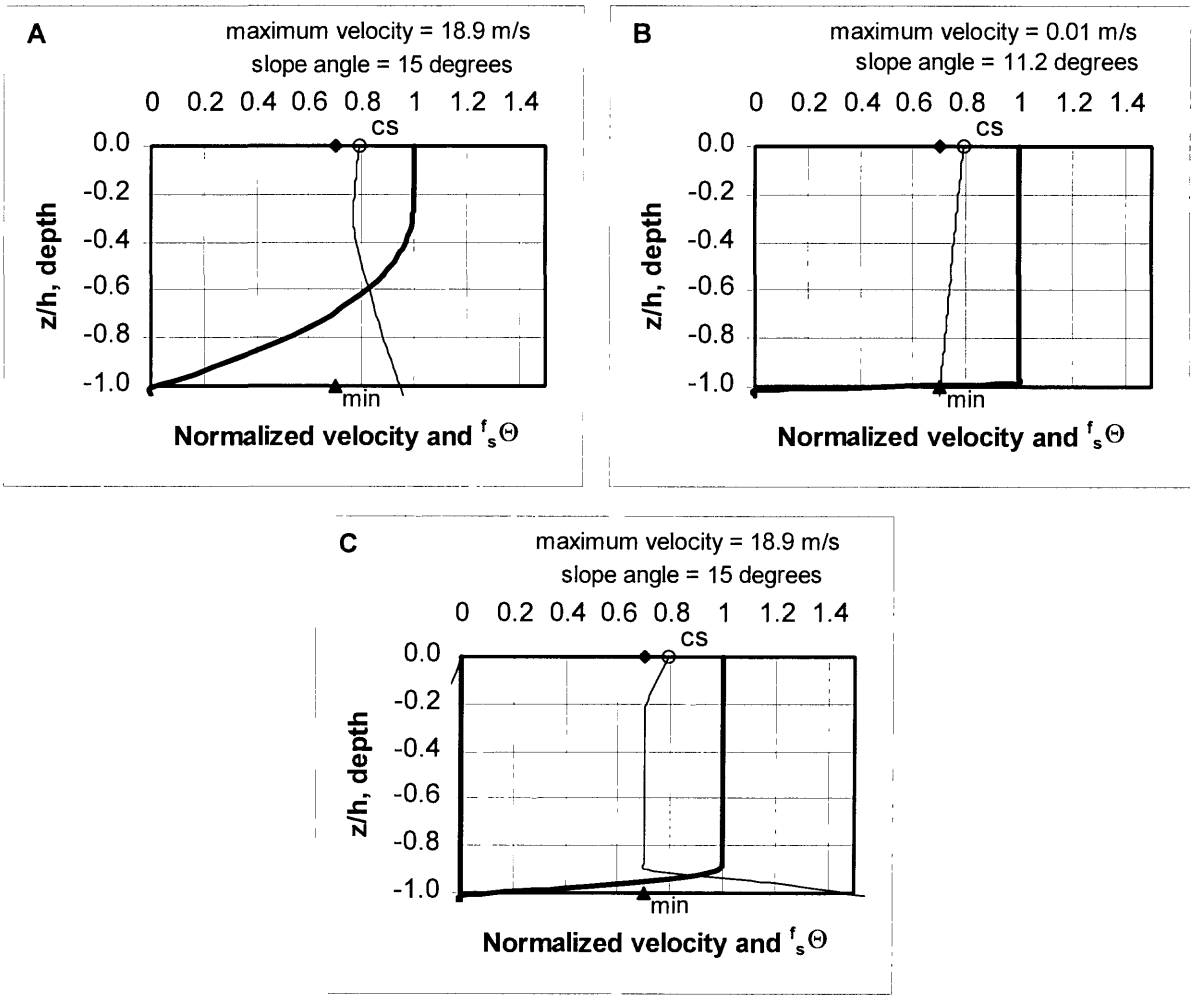

Figure 12. Theoretical velocity profiles for slurry-sand, simple debris-flow materials, using material properties determined experimentally. Thick curve is velocity profile, which is convex throughout depth. Thin curve is volumetric ratio of fluid to solid, $^{sl}_{s}\Theta$. Thickness of flow 0.1 m. Volumetric ratio of slurry fluid phase was $^{w}_{cl}\Theta$ = 14. Dimensionless dispersion coefficient of Λ^* = 2.8. The dispersive coefficient and the pressure coefficient are the same as those used to analyze grain-flow in Figure 11, except the pressure coefficient was reduced by only a factor of five, not ten, for part C. A. The simple debris is flowing down a relatively steep channel, at a slope angle of 15°. The maximum velocity is 19 m/sec. There is a distinct plug, above. This profile is similar to that of an undrained debris flow shown in, but the maximum velocity and slope angle are much larger for the drained flow considered here. B. At the lower slope angle of 11.2°, the flow is nearly all plug, and the flow is essentially sliding on the channel bottom. The maximum velocity is only 0.01 m/sec. C. For the profile shown here, the pressure coefficient has been reduced by a factor of five, and the debris markedly disperses near the base, so the debris still is essentially sliding, but it is sliding at a much higher rate, about 18 m/s.

slope angle (Figure 11A) to disperse the sand grains so that the volumetric ratio of fluid to sand increases with increasing depth. The shearing rate is inadequate for the lower slope angle (Figure 11B) to maintain dispersion of the grains below a certain depth so the volumetric ratio of fluid to sand ${}^{w}_{s}\Theta$ decreases there and the sand eventually locks. Only the upper part of the flow can continue.

The different effects of the pressure coefficient and the dispersion coefficient can be visualized by keeping the dispersion coefficient, Λ^*, high at 2.8, but lowering the pressure coefficient α^* by an order of magnitude to 1.0, as in Figure 11C. A slope for which flow occurs is 6.6°. As a result of the low pressure coefficient, the volumetric concentration of fluid ${}^{w}_{s}\Theta$ decreases abruptly from the value of the critical state at the surface to the minimum value at a shallow depth and throughout the strength plug. The entire upper part of the flow is a strength plug. At the base of the plug, as a result of the high dispersion coefficient, the volumetric concentration of fluid increases and the velocity gradient increases, so the lower part of the flow becomes a zone of high shearing. The velocity of the plug is high, about 37 m/s.

Thus the pressure coefficient determines how quickly the volumetric concentration of fluid ${}^{w}_{s}\Theta$ decreases with overburden pressure whereas the ratio of the dispersion coefficient and the pressure coefficient determines how much the volumetric concentration of fluid increases with rate of shearing deformation.

Note that there are two interesting consequences of this combination of high dispersion coefficient and low pressure coefficient. First, the slope angle, β, must be a little higher for flow to occur at all when the pressure coefficient is low. With the lower pressure coefficient, the minimum slope angle is about 6.4°, whereas with the higher pressure coefficient, flow occurred on a slope of 4° (Figure 11B). Second, the dispersion is very high near the base of the flow where the ratio of fluid to solid ${}^{w}_{s}\Theta$ reaches the high value of more than 1.4 (Figure 11C). As a result, there is a deep strength plug, no sediment plug and a thin zone of intense shearing. The strength plug scoots along quickly on the thin zone of shearing at the base of the flow. For a slope angle of 6.6° the maximum velocity is 37 m/s. For a slope angle of 6.8°, the maximum velocity doubles, to about 70 m/s.

Debris Flow

We have seen that the effect of drainage of the pore fluid and the resultant dissipation of pore-fluid pressures has a marked effect on the flow of grain-flow materials. The same is true for simple debris, consisting of sand and a fluid phase of clay and water. We have analyzed the flow of simple debris containing dilute slurry under drained conditions. We emphasize, though, that drained conditions should pertain to debris flow only if a debris flow is moving quite steadily through a channel, without mixing, so that the excess pore pressures developed deep in the flow can dissipate. Figure 12 shows a solution for drained flowage of simple debris with highly fluid slurry. The mixtures of sand and slurry at various depths in the flows have the properties determined experimentally with the rolling-sleeve apparatus, so that $\eta^* = 0.13$; $\tau^*_0 = 0.004$, $\gamma^* = 0.42$. Again, we assume values for the dispersion coefficient, Λ_2 and the pressure coefficient, α, in dimensionless numbers. As with the sand-water mixtures, we assume a dispersion coefficient of $\Lambda^* = 2.8$ and a pressure coefficient of $\alpha^* = 10$.

Figure 12A shows a velocity profile for a sand-slurry debris flow with a thickness of $h = 0.1$ m flowing down a slope inclined at an angle of $\beta = 15°$. The entire thickness of the debris is flowing, but there is a distinct, strength plug above, about 0.04 m thick, which closely resembles the plugs in debris flows (Figure 9B). Below the plug, the velocity distribution closely resembles that of a viscous fluid. The distribution of volumetric ratios of fluid to solid is shown with the thin line. The ratio decreases slightly within the plug, from the critical state value of ${}^{sl}_{s}\Theta_{cs} = 0.78$ at the surface to about 0.75 at the base of the plug, and then increases within the shearing debris to about 0.85 at the base of the flow.

This profile closely resembles that for simple debris flowing under undrained conditions, and shown in A, but the slope angle and the maximum velocity are much higher. For the undrained flow the slope angle is 10° and the maximum velocity is a docile 4.9 m/s. For the drained flow the slope angle is 15° and the maximum velocity is 19 m/s.

Figure 12B shows the same debris, with the same parameters, flowing down a channel with a shallower slope of $\beta = 11.2°$. The strength plug is much thicker, comprising most of the depth of the flow. The maximum velocity is low, about 0.01 m/s. The slope angle of 11.2° is the minimum slope angle for flow—sliding really—of the debris. Another

difference is visible in the distribution of volumetric ratios of slurry to sand, ${}^{sl}_{s}\Theta$. In the more steeply sloping channel, the velocity gradient below the plug was high enough to disperse the sand, and the dispersion increased with depth. In the more shallowly sloping channel the sand consolidated, reducing the volumetric ratio of slurry to sand from the critical–state value of 0.79 at the surface to the minimum value of 0.7 at a depth near the base of the flow. Near the base of the flow, though, the shear stress became great enough to deform the mixture and flow occurred within a thin film or layer near the base of the flow, much like a fault.

Figure 12C shows the same debris except the dimensionless pressure coefficient α^* has been reduced from 10 to 2. The maximum velocity is about 18 m/s. As a result of the lower pressure coefficient, the debris disperses markedly near the base of the flow, producing a thin shear zone that accommodates rapid translation of the strength plug. The slope angle is somewhat lower, 13°, but the velocity is about the same as high as that in the flow shown in Figure 12A on a 15° slope.

CONCLUSIONS

A combination of the macro–viscous model for the viscosity of simple debris (Johnson, 1965, 1970, 1984; Rodine and Johnson, 1976; Martosudarmo and Johnson, 1997) and Bagnold's inertial model for the inertial behavior of dry granular solids, as developed by McTigue (1982), can account for the rheological properties of a relatively wide variety of mixtures of water, clay and sand. The combined model should be given further consideration in studies of grain flows, debris avalanches and debris flows because it provides a unified approach to the description of the rheology of the masses involved in these different processes. The model accounts well for effects of changes of viscosity and strength of the fluid phase as well as changes in concentration of the granular phase, at least for quartz silt, medium–grained quartz sand and fine–grained plastic beads with the density of water.

A McTigue–Bagnold number is introduced as a criterion for distinguishing conditions under which macro–viscous and inertial behaviors predominate. Our experimental measurements and calculations of McTigue–Bagnold numbers as functions of concentration of grains indicate that inertial effects will predominate if deformation rates are greater than about 10/sec for grain flows with volumetric ratios of water to medium–grained sand of ${}^{f}_{s}\Theta = 0.8$ and greater than about 22/sec at ${}^{f}_{s}\Theta = 1.0$. For dilute slurry, with a viscosity about 15 times that of water and a strength of 3 Pa, deformation rates must be 3 to 6 times higher for inertial effects to predominate. Deformation rates must be greater than about 30/sec for ${}^{f}_{s}\Theta = 0.8$ and 120/sec at ${}^{f}_{s}\Theta = 1.0$.

Solutions for flow of the grain–flow mixtures of sand and water and simple debris–flow mixtures of sand and slurry indicate that the velocity profiles should be quite different for these two types of materials. Indeed, the velocity profiles for reasonable solutions for the grain flows indicates the characteristic doubly curved, convex upper and concave lower profile, with a small strength plug at the flow surface. In this respect, the profiles are similar to those obtained by Takahashi (1991) and Chen (1987) for mixtures of granular solids and water (e.g., Figure 9A). The velocity profiles for reasonable solutions for simple debris have the characteristic singly curved, convex profile, with a bold plug. These profiles are thus similar to the profiles that characterize debris flows, as for example the one shown in Figure 9B.

The research reported here goes a long way toward re–orienting our early research on debris flow. According to a critical review of mechanical analyses of debris flow by Iverson and Denlinger (1987), a definite weakness of our early work was the focus on the *statics* of debris flow at the expense of ignoring the dynamics. According to Iverson and Denlinger, the viscoplastic conceptualization of debris flows . . . "is founded largely on the idea that a continuous, muddy, matrix phase gives the debris both strength and viscosity, and these matrix properties control the mechanical behavior of the flow." Furthermore,

> the fundamental shortcoming of the viscoplastic debris–flow theory is that it makes no provision for dynamic particle interactions with one another or with the fluid–like matrix. Such interactions are obvious to field observers [of debris flows] . . . Thus . . . the viscoplastic theory is at best incomplete. A more [nearly] complete theory would explain observations that the viscoplastic theory explains, and . . . would also account for the interactions of discrete debris–flow constituents.

Iverson and Denlinger point out that the vertical profiles for debris flows computed with Bagnold's model or with various modified versions of Bagnold's model assumed by Takahashi (e.g., 1980, 1991) and Chen (e.g., 1987), have a peculiar

concave–upward slope (Figure 9A), which does not simulate the rigid plug that characterizes debris flow (Figure 9B). Iverson and Denlinger conclude that, although the uniformly–dispersed grain–flow model, such as that suggested by Chen and Takahashi, has apparent advantages over the Terzaghi–Coulomb–viscous model, the assumption that the matrix behaves as an ideal fluid, with negligible viscosity, is a significant shortcoming.

The combined macro–viscous and inertial model that was initiated with Rodine's (1974) research and continued with McTigue's (1979) and Martosudarmo's (1994) research, culminating in the viscous–inertial model presented here, seems to provide the new direction required to develop viable models of debris flow, grain flow and debris avalanche. On the basis of this model, we can understand how the concept of debris flow can include a wide range of natural phenomena.

Pierson and Costa (1987) and Fleming and Varnes (1991) have recognized that the different mechanisms reflected in the Terzaghi–Coulomb–viscous model, on one hand, and the Bagnold model, on the other, are reflected in different natural phenomena that are lumped under the general designation of *debris flow.* In a *debris avalanche,* which initiate on high, steep slopes, the debris is shearing at such a high rate that the resistance due to impact of clasts dominates over resistance due to strength and viscosity of the interstitial fluid of the debris. In this view, the inertial viscosity would much larger than the macro viscosity in debris avalanches. I believe that the phenomena investigated by Takahashi and his associates in Japan are grain flows and debris avalanches, not muddy debris flows.

Muddy debris flows are much less violent, and they typically initiate from landslide masses (Johnson, 1984; Fleming and others, 1989). In muddy debris flows the macro viscosity is larger than the inertial viscosity.

Muddy debris can remain mobile even if the debris is flowing slowly. This is a result of the astonishingly low conductivity of the granular phase of a debris flow with respect to the mixture of clay and water in the interstices of the granular phase and the low conductivity of water with respect to the solids.

The distinction between highly–energized debris flows, in the form of debris avalanches, and docile debris flows, in the form of muddy debris flows, is quite significant, because an avalanche tends to be catastrophic, whereas a flow tends to be relatively deliberate. The difference in dynamics between these two kinds of flow was recognized by Plafker and Ericksen (1978), who described a spectacular debris avalanche in Peru that reached extremely high speeds as it, essentially, fell down a steep mountain front, then transformed into a much–milder debris flow on lower slopes.

The concept of debris flow, though, spans the range of these phenomena according to Pierson, Costa, Fleming and Varnes.

ACKNOWLEDGMENTS

I have worked closely, first with Yanto Martosudarmo and then with Bill Schulz, on the research reported here. I have also gained from discussions and experiments conducted with Jeff Tropp, Rick Hoy and Ken Ridgway. I thank them for the collaboration. Robert Fleming listened politely and was generally enthusiastic as I told him about progress of the research. I thank him for his support. I am grateful to William Savage, U. S. Geological Survey, for a careful review. I am grateful to James Gardner, Technical Editor of Earth and Atmospheric Sciences at Purdue, for improving the writing. This research was not funded by any agency, although I used earthquake research funds to buy laboratory supplies. For this unofficial support I am grateful to NSF and DOE. I accept sole responsibility, however, for the shortcomings of the research and this presentation.

REFERENCES CITED

Bagnold, R.A., 1936. The movement of desert sand. Proc. Roy. Soc. of London, Ser. A., 157:594–619.

Bagnold, R.A., 1941. The physics of blown sand. London, Metheun.

Bagnold, R.A., 1954. Experiments on a gravity–free dispersion of large solid spheres in a Newtonian fluid under shear. Proc. Roy. Soc. of London, Ser. A., 225:49–70.

Bagnold, R.A., 1956. The flow of cohesionless grains in fluids. Proc. Roy. Soc. London, Ser. A. , 249, 235–297.

Bagnold, R.A., 1966. We Need This Reference.— Proc. Royal Soc. London, Ser. A., 295:219–232.

Bagnold, R.A., 1980. An empirical correlation of bedload transport rates in flumes and natural rivers: Proc. Royal Soc. London, ser. A, 372:453–473.

Bear, J., 1972. Dynamics of fluids in porous media. American Elsevier Publishing Co., N.Y. [reprinted by Dover Publications, 1988], 764 p.

Campbell, C.S., 1989. The stress tensor for simple shear flows of granular material. Jour. Fluid Mech., 203:449–473.

Campbell, C.S., and Brennen, C.E., 1985. Chute flows of granular material: some computer simulations, Jour. Appl. Mech., 52:172–178.

Chen, C., 1985. Present status of research in debris flow modeling. In, Proc. Hydraul. Div. Specialty Conf. on Hydraulics and Hydrology in the Small Computer Age: Lake Buena Vista, Florida, American Soc. Civ. Engrs, 733–741.

Chen, C., 1987. Comprehensive review of debris flow modeling in Japan, in Costa, J.E. and Wieczorek, G.F., Debris flows/avalanches: Process, recognition, and mitigation. Geol. Soc. Am. : Review in engineering geology, vol. 7:13–30.

Chen, C., 1988. Generalized viscoplastic modeling of debris flow. Jour. Hydraulic Engrg., ASCE, 114:237–257.

Cowin, S.C., 1974. A theory for the flow of granular materials. Powder Tech., 9:61–69.

Cowin, S.C., 1978. Microstructural continuum models for granular materials. Proc. U.S.–Japan Seminar on Continuum Mechanical and Statistical Approaches in the Mechanics of Granular Materials. Cowin, S.C., and Satake, M., eds., akujutsu Bunken Fukyui–kai, Tokyo, p. 162–170.

Fleming, R.W., Ellen, S.D., and Algus, M.A., 1989. Transformation of dilative and contractive landslide debris into debris flows-and example from Marin County, California., Engineering Geology, 27: 201-224.

Goodman, M.A., and Cowin, S.C., 1971. Two problems in the gravity flow of granular materials. Jour. Fluid Mech., 45:321–339.

Iverson, R.M., and Denlinger, R.P., 1987. The physics of debris flows – a conceptual assessment, In, Beschta, R.L., and others, eds., Erosion and sedimentation in the Pacific rim. International Association of Hydrological Sciences, Publ. no 165:155–165

Johnson, A.M., 1965. A model for debris flow. Ph.D. dissertation, Pennsylvania State University, Univ. Park, Penna.

Johnson, A.M., 1970. Physical Processes in Geology. Freeman, Cooper & Co., San Francisco, 577 p.

Johnson, A.M., 1984. Debris flow. In, Brunsden, D., and Prior, D.B. (Eds.), Slope Instability. John Wiley and Sons, Ltd, New York, 257–361.

Johnson, A.M., and Hampton, M.A., 1968. Subaerial and subaqueous flow of slurries—An investigation of processes of turbidity–current flow and debris flow. Annual Progress Report, Contract no. 14–08–0001–10884, U.S. Geological Survey. Branner Library, Stanford University, 56 p.

Johnson, A.M., and Hampton, M.A., 1969. Subaerial and subaqueous flow of slurries. Final Report to U.S. Geological Survey Contract No. 14–08–001–10884.

Johnson, A.M., and Martusudarmo, S.Y., 1997). Discrimination between inertial and macro-viscous flows of fine-grained debris with a rolling-sleeve viscometer. 1st International Conference on Debris–flow Hazards Mitigation: Mechanics, Prediction and Assessment, 7–9 August 1997, Hyatt Regency, San Francisco, California.(Manuscript).

Johnson, A.M., and Rahn, P.H., 1970. Mobilization of debris flows. Zeitschrift fur

Geomorphologie, Supplemant band 9:168–186.

Martosudarmo, S. Y., 1994. Flow properties of simple debris. Ph.D. dissertation, Purdue University, 199 p.

Martosudarmo, S.Y., and Johnson, A.M.,1997. Ability of muddy debris to remain mobile at low flow rates. 1st International Conference on Debris–flow Hazards Mitigation: Mechanics, Prediction and Assessment, 7–9 August 1997, Hyatt Regency, San Francisco, California (Manuscript).

McTigue., D.F., 1979. A nonlinear continuum model for flowing granular materials. Ph.D. dissertation, Stanford University, 165pp.

McTigue, D.F., 1982. A nonlinear constitutive model for granular material: Application to gravity flow. Journal of Applied Mechanics, vol. 49. p. 291–296.

Miln, W.E., 1949, Numerical Calculus. Princeton Univ. Press, Princeton, N.Y., 393 pp.

Passman, S.L., Jenkins, J.T., and Thomas, J.P., Jr., 1978. Flow of a granular material in a vertical channel. Proc. U.S.–Japan Seminar on Continuum Mechanical and Statistical Approaches in the Mechanics of Granular Materials. Cowin, S.C., and Satake, M., eds., akujutsu Bunken Fukyui–kai, Tokyo, p. 171–180.

Pierson, T.C., and Costa, J.E., 1987. A rheological classification of subaerial sediment–water flow, in Costa, J.E. and Wieczorek, G.F., Debris flows/Avalanches: Process, recognition, and mitigation. Geol. Soc. Amer. Reviews in engineering geology, vol. 7:1–12

Plafker, G., and Ericksen, G.E., 1978. Nevados Huascaran avalanches, Peru. In, Voight, B., Ed., Rockslides and avalanches. Elsevier Sci. Pub. Co., New York, p.277–314.

Rivlin, R.S., 1947. The hydrodynamics of non–Newtonian fluids. Proc. Roy. Soc. London, Ser. A, 193:260–281.

Rivlin, R.S., 1948. Large elastic deformations of isotropic materials, I. Fundamental concepts. Philosophical Transactions of the Royal Society of London, Series A 240:459–490.

Rivlin, R.S., 1951. Large elastic deformations of isotropic materials, VII. Further developments of the general theory. Philosophical Transactions of the Royal Society of London, Series A 241:379–397.

Rodine, J. D., and Johnson, A.M., 1976. The ability of debris heavily freighted with coarse clastic materials to flow on gentle slopes. Sedimentology, 23:213–224.

Rodine, J.D., 1974. Analysis of the mobilization of debris flows. Ph.D. dissertation, Stanford University, Stanford, California, 226 p.

Savage, S.B., 1979. Gravity flow of cohesionless granular materials in chutes and channels. Jour. Fluid Mech., 92:53–96.

Schulz, W.H., 1996. Characteristics of pyroclastic flows deduced from studies of eyewitness accounts of pyroclastic flows and detailed maps of deposits at Mount Saint Helens. M.S. thesis, Anderson and Flett Volcanic Hazard Laboratory, Department of Earth and Atmospheric Sciences, Purdue University, 76 p.

Tadros, T.F.,1987. .Assessment of the properties of suspensions In, Tadros., T.F., ed., *Solid/liquid dispersions.* Academic Press, N.Y. 293–328.

Takahashi, T., 1977. A mechanism of occurrence of mud–debris flow and their characteristics in motion: Kyoto University, Kyoto, Japan, Disaster Prevent Research Institute Annuals, 20–B2:405–435 (in Japanese).

Takahashi, T., 1978. Mechanical characteristics of debris flow. Journal of the Hydraulic Div. ASCE, v. 104:1153–1169.

Takahashi, T., 1980. Debris flow in prismatic open channels. Journal of the Hydraulic Div. ASCE, v. 106:381–396.

Takahashi, T. , 1991. *Debris Flow.* AA Balkema, Rotterdam, 165 pp.

Takahashi, T., Nakagawa, H., and Kuang, S., 1987. Estimation of debris flow hydrograph on varied slope bed. In, Beschta, R.L., and others, eds., Erosion and sedimentation in the Pacific rim. International Association of Hydrological Sciences, Publ. no 165:167–177.